Clim. Past Discuss., 5, 2497–2554, 2009
www.clim-past-discuss.net/5/2497/2009/

Climate of the Past Discussions

A synthesis of marine sediment core $\delta^{13}C$ data over the last 150 000 years

K. I. C. Oliver[1,2], B. A. A. Hoogakker[3], S. Crowhurst[3], G. M. Henderson[4], R. E. M. Rickaby[4], N. R. Edwards[1], and H. Elderfield[3]

[1]Department of Earth and Environmental Sciences, The Open University, Walton Hall, Milton Keynes MK7 6AA, UK
[2]School of Ocean and Earth Science, National Oceanography Centre, University of Southampton, European Way, Southampton SO14 3ZH, UK
[3]Department of Earth Sciences, University of Cambridge, Downing Street, Cambridge CB2 2EQ, UK
[4]Department of Earth Sciences, University of Oxford, Parks Road, Oxford OX1 3PR, UK

Received: 19 November 2009 – Accepted: 21 November 2009
– Published: 11 December 2009

Correspondence to: K. I. C. Oliver (k.i.c.oliver@noc.soton.ac.uk)

Published by Copernicus Publications on behalf of the European Geosciences Union.

Abstract

The isotopic composition of carbon, δ^{13}C, in seawater is used in reconstructions of ocean circulation, marine productivity, air-sea gas exchange, and biosphere carbon storage. Here, a synthesis of δ^{13}C measurements taken from foraminifera in marine sediment cores over the last 150 000 years is presented. The dataset comprises previously published and unpublished data from benthic and planktonic records throughout the global ocean. Data are placed on a common δ^{18}O age scale and filtered to remove timescales shorter than 6 kyr. Error estimates account for the resolution and scatter of the original data, and uncertainty in the relationship between δ^{13}C of calcite and of dissolved inorganic carbon (DIC) in seawater. This will assist comparison with δ^{13}C of DIC output from models, which can be further improved using model outputs such as temperature, DIC concentration, and alkalinity to improve estimates of fractionation during calcite formation.

High global deep ocean δ^{13}C, indicating isotopically heavy carbon, is obtained during Marine Isotope Stages (MIS) 1, 3, 5a, 5c and 5e, and low δ^{13}C during MIS 2, 4 and 6, which are temperature minima, with larger amplitude variability in the Atlantic Ocean than the Pacific Ocean. This is likely to result from changes in biosphere carbon storage, modulated by changes in ocean circulation, productivity, and air-sea gas exchange. The North Atlantic vertical δ^{13}C gradient is greater during temperature minima than temperature maxima, attributed to changes in the spatial extent of Atlantic source waters. There are insufficient data from shallower than 2500 m to obtain a coherent pattern in other ocean basins. The data synthesis indicates that basin-scale δ^{13}C during the last interglacial (MIS 5e) is not clearly distinguishable from the Holocene (MIS 1) or from MIS 5a and 5c, despite significant differences in ice volume and atmospheric CO_2 concentration during these intervals. Similarly, MIS 6 is only distinguishable from MIS 2 or 4 due to globally lower δ^{13}C values both in benthic and planktonic data. This result is obtained despite individual records showing differences between these intervals, indicating that care must be used in interpreting large scale signals from a small

number of records.

1 Introduction

The isotopic composition, $\delta^{13}C$, of inorganic carbon in seawater is a diagnostic of ocean circulation and the marine and terrestrial carbon cycle. The potential for $\delta^{13}C$ in calcium carbonate shells, formed by foraminifera and preserved in marine sediments, to record past changes in climate has been recognised since the 1970s (Shackleton, 1977; Duplessy et al., 1981). Greater differences in $\delta^{13}C$ between planktonic and benthic foraminifera, during glacial periods, were interpreted as indicating greater storage of isotopically light organic carbon in the deep ocean and linked to atmospheric pCO_2 (Broecker, 1982a; Shackleton et al., 1983; Shackleton et al., 1992). Lower $\delta^{13}C$ values recorded in the Pacific Ocean, during the last glacial maximum (LGM), were attributed to a change in the ocean $\delta^{13}C$ reservoir due to the release of organic carbon from the terrestrial biosphere or marine shelf sediments (Broecker, 1982b; Duplessy et al., 1988b). Carbon isotopes have also been used to reconstruct past water masses, notably low $\delta^{13}C$ Antarctic source waters and high $\delta^{13}C$ Atlantic source waters (Sarnthein et al., 1994), or to diagnose changes in air-sea gas exchange (Marchitto and Broecker, 2006). However, the interpretation of the $\delta^{13}C$ is complicated by the dependence of fractionation during calcification on properties of the water (temperature; $[CO_2]$; $[CO_3^{2-}]$) and the foraminifer (species; shell size; diet), and on the formation of microenvironments around benthic foraminifera (Sect. 3). The variety of mechanisms influencing the $\delta^{13}C$ record is summarised in Fig. 1.

The reconstruction of past ocean states depends on the collation of $\delta^{13}C$ observations from throughout the ocean, which can provide a fairer test to hypotheses than individual datasets. The demand for such syntheses is increased by the development of Earth system models that are able to simulate paleoclimate proxies including $\delta^{13}C$ (Ridgwell et al., 2007; Brovkin et al., 2007). Previous data syntheses have consisted of timeslices for selected regions such as the Atlantic Ocean (Sarnthein et al., 1994;

Bickert and Mackensen, 2003; Curry and Oppo, 2005; Lynch-Stieglitz et al., 2007), typically focusing on the difference between the late Holocene and the LGM. Data from the benthic species *Cibicidoides wuellerstorfi*, considered the most reliable indicator of seawater δ^{13}C, were selected for those time-slices, reducing the error in the data at the expense of reduced data coverage. In this study, we focus not on specific timeslices but on producing a synthesis of timeslices, at 2 kyr intervals, for the last 150 kyr. We include data from a range of benthic and planktonic species, and do not exclude data from high productivity regions. The inhomogeneity in this data is addressed by attaching an error estimate for each observation, using the entire dataset to estimate additional errors associated with less reliable species and unfavourable core locations.

The goals for this study are threefold: (1) to provide a common δ^{18}O-derived age-scale for a synthesis of δ^{13}C data; (2) to provide δ^{13}C error estimates for the synthesis, in order to facilitate direct model–data comparison; (3) to provide a global overview of the data, and an account of the large scale processes invoked to explain changes in ocean δ^{13}C. In Sect. 2, we introduce the data and summarise the age-scale introduced in the companion paper (Hoogakker et al., 2009a). In Sect. 3, we describe the methods used to determine uniformly spaced time-series and uncertainty intervals. In Sect. 4, we examine δ^{13}C time-series, grouped by region, and six time-slices, as well as planktonic-benthic differences. We summarise our findings in Sect. 5, and discuss their application for Earth System models and biosphere reconstructions.

2 Data

2.1 Data selection and coverage

Table 1 summarises the data used in this compilation. Data consist mostly of records submitted to the PANGAEA publishing network for geoscientific and environmental data (http://pangaea.de), the National Geophysical Data Centre (NGDC; http://www.ngdc.noaa.gov), or the Delphi Project (http://rock.esc.cam.ac.uk/delphi), with additional records obtained through personal correspondence. $\delta^{13}C$ records were accepted into the pre-processed compilation provided that it was possible to obtain a reliable (though sometimes low resolution) age model within the last 150 000 years using $\delta^{18}O$ stratigraphy (Hoogakker et al., 2009a). No data quality constraint was applied to the pre-processed compilation, but several factors (detailed in Sect. 3) can lead to a large error estimate, so that some data were ultimately rejected as having too large an associated error to be useful.

Figure 2 shows the core locations for the records used in the data synthesis, as well as for records for which we were unable to provide a $\delta^{18}O$–derived age model. Among the records that were used, there is good data coverage in deep waters (>2500 m) in the Atlantic Ocean (100 cores with benthic data). Atlantic data coverage is also reasonable at shallower depths (45 cores) and in surface waters (71 cores with planktonic data). The principal gaps in benthic data coverage are: (1) <2500 m in the Pacific ocean (10 cores); (2) the Indian ocean (12 cores); and (4) south of 50° S (2 cores). There is a large variation in the temporal resolution of the pre-processed data, both within and across cores. Of the cores providing benthic data, all but 28 provide at least one observation for the LGM (19–23 ka), compared with 64 cores providing no Holocene (<10 ka) data, and 124 cores providing no data from Marine Isotope Stage (MIS) 5a or earlier (>71 ka). This is summarised in Table 1. The data, pre-processed onto a $\delta^{18}O$ age-scale and with a limited amount of filtering (the exclusion of small subsets of data taken from a different species to the majority of the record) but with no changes to $\delta^{13}C$ values, are available from the authors. We caution that these data do not constitute a repository of raw records, which can instead be obtained from PANGAEA, NGDC, or Delphi. The fully processed data, after applying the methods described in Sect. 3, are included as Supplementary Materials http://www.clim-past-discuss.net/5/2497/2009/cpd-5-2497-2009-supplement.zip.

2.2 Age modelling

A detailed description of the age modelling method is provided in the companion paper (Hoogakker et al., 2009a). In summary, $\delta^{18}O$ data, obtained together with $\delta^{13}C$ data, were used to manually obtain pivot dates at 18 ka, 62 ka, 87 ka, 108 ka, and 137 ka. It was assumed that these dates correspond to local maxima in the $\delta^{18}O$ time-series. The selection of these pivot dates was constrained by a subjective judgement of plausible age-depth relationships; large changes in mean sedimentation rate between pivot dates were considered unlikely, though not impossible. Between pivot-points, a uniform sedimentation rate was assumed. For high resolution records where pivot dates could be clearly identified, we estimate 2σ uncertainties associated with this approach of up to 6 kyr between pivot dates (excluding uncertainties in the initial selection of dates of $\delta^{18}O$ maxima). Lower resolution cores, cores with low resolution segments (see Table 1), or cores with hiatuses, are likely have greater dating uncertainties. Therefore inter-basin differences in the timing of $\delta^{18}O$ changes (Skinner and Shackleton, 2005) are unlikely to be a major additional source of dating error. The age models presented are not suitable for examining the detailed phasing of changes in $\delta^{13}C$ within deglaciations, or for events with timescales close to that of ocean circulation, but are suitable for examining variability on orbital timescales.

Earlier published or unpublished age models, based on a variety of methods including radiocarbon dating and stratigraphy, were also obtained for many of the records. In many cases, they provide more accurate and well-resolved age records than the $\delta^{18}O$ timescale used in this study. However, this is not universally the case, and we caution that they provide a large range of estimates for the dating of events such as the LGM and the last interglacial, due to the variety of methods used.

3 Procedure for temporal gridding and $\delta^{13}C$ uncertainty estimation

This section describes the treatment of data inhomogeneity within and between records in obtaining a temporally gridded data synthesis, with uncertainties ascribed to individual $\delta^{13}C$ values as a function of species, core location, data resolution and scatter. In accounting for data inhomogeneities, it is useful to distinguish between systematic errors associated with each record (inter-record error) and the temporally varying error component (intra-record error). For example, the error due to fractionation during calcification has a large inter-record component because this is strongly dependent on species, and most records consist of samples from a single species or genus. Spatial variability in the species offset is also an inter-record error, but in situ variability of this offset in response to climate change is an intra-record error. Similarly, any systematic difference in $\delta^{13}C$ resulting from inter-laboratory calibration errors is an inter-record error. Since we expect uncertainties in the systematic inter-record error to be significant, $\delta^{13}C$ and its uncertainties are estimated by two stages. First, we present intra-record variability in $\delta^{13}C$ relative to the LGM, which we label $\Delta_{LGM}\delta^{13}C$ (Sect. 3.1). Second, we obtain estimates for absolute $\delta^{13}C$ values (Sect. 3.2). $\Delta_{LGM}\delta^{13}C$ can be used to understand spatial patterns in $\delta^{13}C$ variability, and has smaller uncertainty than absolute $\delta^{13}C$. Therefore, we recommend that $\Delta_{LGM}\delta^{13}C$ is chosen where possible when using this data synthesis (for example for model-data comparison), and it is also the variable presented in most figures within this paper.

3.1 Obtaining $\delta^{13}C$ as anomalies relative to the LGM

$\Delta_{LGM}\delta^{13}C$ is temporally gridded at 2 kyr intervals, and the smoothing spline applied to the data approximates a 6 kyr low pass filter (Sect. 3.1.1), removing high frequency variability such as Dansgaard-Oeschger oscillations which are beyond the precision of the age model. All $\Delta_{LGM}\delta^{13}C$ values are calculated as an anomaly relative to the LGM. This is defined at 21 ka, providing a good approximation to the common LGM definition of 19–23 ka (e.g. Bickert and Mackensen, 2003; Paul et al., 2009); averaging pre-processed data within the 19–23 ka interval would not be preferable due to uncertainties in the age model. The LGM, rather than the late Holocene, is chosen as the reference period because almost all cores provide LGM data, whereas approximately half of all cores provide no data for <4 ka.

Three steps were taken to obtain $\Delta_{LGM}\delta^{13}C$ estimates and uncertainties, described in detail below. First, each time-series was smoothed and gridded, and the error associated with this process estimated (Sect. 3.1.1). Second, a correction and additional error was estimated for cores thought to be subject to changes in the phyto-detritus effect (Sect. 3.1.2). Third, an error for the representativeness of each species of the ambient water was estimated (Sect. 3.1.3). Although the errors associated with each of these steps are likely to be correlated, there were insufficient data to reliably estimate these correlations, so the total error was estimated to be the quadratic sum of the error components. 2σ error estimates are quoted; where they exceed 1‰ or where the data resolution is poorer than 6 kyr, no final $\Delta_{LGM}\delta^{13}C$ estimate is given. Full error estimates are provided as part of the uniformly spaced output dataset (Supplementary Materials http://www.clim-past-discuss.net/5/2497/2009/cpd-5-2497-2009-supplement.zip).

3.1.1 Smoothing splines

The first step in obtaining $\Delta_{LGM}\delta^{13}C$ estimates was independent of species or region, and a function only of the input time-series data. These were smoothed and placed on a uniform 2 kyr grid using the spline smoothing method described by Silverman (1985). For a time-series of n observations, the set of $n-1$ cubic equations was obtained which minimised

$$\theta = \lambda \int_{t_1}^{t_n} \ddot{y}^2 \mathrm{d}t + n^{-1} \Sigma_{i=1}^{n} y_i'^2, \tag{1}$$

where λ is the smoothing parameter, y is the output $\delta^{13}C$ estimate and $\ddot{y}$ is its second derivative with respect to time, t_1 and t_n are dates for the top and bottom, respectively, of each record (note that t is defined positive towards the past), and y' is given by

$$\begin{aligned} y_i'^2 &= (y_i - Y_i)^2, \quad |y_i - Y_i| \le y_{\mathrm{thr}}, \\ y_i'^2 &= y_{\mathrm{thr}}^2 + |y_i - Y_i| - y_{\mathrm{thr}}, \quad |y_i - Y_i| > y_{\mathrm{thr}}, \end{aligned} \tag{2}$$

where Y_i is the δ^{13}C observation and y_{thr}=0.5‰ was chosen to prevent outliers from having a dominant effect on the estimate (Enting, 1987). The smoothing parameter is given by

$$\lambda = \frac{(n-1)T_{0.5}^4}{(2\pi)^4(t_n - t_1)}, \tag{3}$$

where $T_{0.5}$ was chosen to be 6 kyr. For a uniformly spaced input time-series, this method is equivalent to a kernel filter admitting 50% of variability with a period of $T_{0.5}$, steeply increasing towards 100% at longer timescales and steeply decreasing towards 0% at shorter timescales (Enting, 1987). For time-series with non-uniformly spaced data, the period at which 50% of the variability is admitted is a weak function ($\sim \hat{f}^{-\frac{1}{4}}$) of the local kernel density $\hat{f}$. Kernel data density estimates, which approximate to the inverse of the temporally local data resolution Δt, are provided as part of the uniformly spaced output dataset (Supplementary Materials http://www.clim-past-discuss.net/5/2497/2009/cpd-5-2497-2009-supplement.zip).

A first estimate of the error in the smoothed time-series is given by (Silverman, 1985)

$$2\sigma_{\mathrm{sil}}(t) = 2\left(4\lambda^{\frac{1}{3}}\hat{f}(t)\right)^{-\frac{3}{8}} \left(\frac{\Sigma_{i=1}^{n} y_i'^2}{n^{\frac{3}{4}} - 2^{-\frac{3}{2}}\lambda^{-\frac{1}{4}}\Sigma_{i=1}^{n}\hat{f}(t_i)}\right)^{\frac{1}{2}}. \tag{4}$$

Typical values of $2\sigma_{\mathrm{sil}}$ are of the order of 0.1‰, rarely increasing above 0.25‰. However, this method is intended for time-series with large n, and unrealistically small error estimates are produced for time-series with a temporal resolution of the same order as $T_{0.5}$. Enting (1987) noted that an accurate error estimate depends on a knowledge of the spectral characteristics of both the signal and the noise. For our purposes, all high frequency variability is noise, and it is likely that this is aliased in low resolution time-series. In order to address this, we assume that the root-mean-square of the residuals, $\bar{y'}$, from high resolution time-series provides an estimate of the noise present in all time-series. Where smaller values of $\bar{y'}$ are obtained from low resolution records, this indicates that variability in the high frequency ($T < T_{0.5}$) band is being aliased as a signal at lower frequencies. $\bar{y'}$ is plotted as a function of time-series mean resolution in Fig. 3, along with a line of best fit, y'_h, with the form of a *tanh* function. We obtain lower values of y'_h in low resolution cores. The resulting error estimate due to aliasing,

$$2\sigma_\mathrm{ali}(\Delta t) = 2\left(y'_\mathrm{h}(0) - y'_\mathrm{h}(\Delta t)\right)\left(1 + \frac{T_0}{\pi \Delta t}\right)^{-\frac{1}{2}}, \quad (5)$$

is also plotted if Fig. 3. Note that there is a large range in y'_h even within high frequency time-series, likely to be largely caused by data inhomogeneities about which information is often unavailable (e.g. shell sizes used; shells per sample; averaging of duplicate samples). Therefore aliasing error estimates for low resolution time-series are very uncertain. The total error associated with the smoothing spline process is the quadratic sum of $2\sigma_\mathrm{sil}$ and $2\sigma_\mathrm{ali}$.

3.1.2 Error due to the phyto-detritus effect

A further source of error is the possible change in time of the depositional environment in which benthic foraminifera exist. Infaunal species such as those in the *Uvigerina* genus inhabit a microenvironment that is often depleted in δ^{13}C due to the respiration of organic matter in the sediment, whereas δ^{13}C epifaunal species are not typically subject to this effect. There is some evidence that the error in infaunal species varies over a glacial cycle (Hoogakker et al., 2009b), but there are insufficient data to determine a correction that varies over time. In this study, we treat this effect as a constant component of the species offset plus a random error (Sect. 3.1.3); therefore there is no phyto-detritus correction to $\Delta_\mathrm{LGM}\delta^{13}$C in infaunal species.

Although shells from the epifaunal *Cibicidoides* taxon are thought usually to record the $\delta^{13}C$ of ambient water ΣCO_2 accurately, several studies have identified a bias toward low values in high productivity regions (Mackensen et al., 1993; Sarnthein et al., 1994), termed the phyto-detritus effect. Bickert and Wefer (1999) compared cores from upwelling regions in the Atlantic Ocean to nearby cores outside upwelling regions and found that $\delta^{13}C$ in upwelling regions was more depressed, relative to nearby cores, during the LGM than the late Holocene. Bickert and Mackensen (2003) applied a correction of +0.4‰ to LGM $\delta^{13}C$ in several upwelling regions in the Atlantic Ocean (parts of the eastern boundary in both hemispheres; equator; subtropical and subantarctic fronts), applying no analogous correction to Holocene values. Such a time-dependent correction influences both $\delta^{13}C$ and $\Delta_{LGM}\delta^{13}C$ estimates. Figure 4 shows the correction and uncertainty that we add to $\delta^{13}C$ estimates in cores, flagged in Table 1, found in the upwelling regions identified by Bickert and Mackensen (2003), including the Antarctic Circumpolar Current. The correction for the LGM is +0.4‰ and for the late Holocene is zero, with an assumed $2\sigma_{phy}$ error of 0.4‰ at all times. Phyto-detritus corrections, in ‰, throughout the 150 kyr record are given by

$$\delta_{phy}(t) = 0.4\left(1 - \frac{\overline{(\Delta_{LGM}\delta^{13}C)_{S1}}^{phy}(t)}{\overline{(\Delta_{LGM}\delta^{13}C)_{S1}}^{phy}(1\,\mathrm{ka})}\right), \tag{6}$$

where $(\Delta_{LGM}\delta^{13}C)_{S1}$ is the value of $\Delta_{LGM}\delta^{13}C$ obtained after spline fitting but before applying the phyto-detritus correction, 1 ka is chosen to represent the late Holocene, and $\overline{}^{phy}$ indicates averaging over cores for which a phytodetritus correction is applied. Values lower than 0‰ or greater than 0.4‰ are replaced with 0‰ and 0.4‰, respectively. Because the LGM is used as the reference date, the correction towards higher values in glacial $\delta^{13}C$ corresponds to a correction, towards lower values, in interglacial and interstadial $\Delta_{LGM}\delta^{13}C$ (Fig. 4). The 0.4‰ uncertainty is also added to cores at upwelling sites in the Indian and Pacific Oceans (Table 1). However, no correction is applied because there are insufficient data to compare LGM versus Holocene differences at Indo-Pacific upwelling sites to those at nearby sites where there is no upwelling. Therefore, we lack the evidence to support a stronger phytodetritus effect during cold climates in these oceans.

It is not well known to what extent the phyto-detritus effect in epifaunal species is caused by changes in foraminifer growth rate (McConnaughey et al., 1997), or by the build-up of respiring organic matter over epifaunal species leading to a decrease in $\delta^{13}C$ similar to that observed in infaunal species. No correlation has been observed between sedimentation rate and amplitude of the phyto-detritus effect, although Mackensen et al. (2001) suggested that this is because the key control is seasonal peak deposition rate, rather than annual mean deposition rate. It is therefore uncertain whether additional errors are introduced to records from infaunal species in high productivity regions. As noted above, we apply no correction, but add the same uncertainty as would be added to epifaunal species.

3.1.3 Disequilibria and the calculation of species errors

An important error in $\Delta_{LGM}\delta^{13}C$ estimates is variability in disequilibria of $\delta^{13}C$ in calcium carbonate in the shells of foraminifera, relative to the ambient water. Along with the phyto-detritus effect, $\delta^{13}C$ disequilibrium leads to the application of different "species offsets" to $\delta^{13}C$ data collected from different species. We note that $\Delta_{LGM}\delta^{13}C$ is independent of any uniform species offset, and that errors due to variability between individual shells, or small groups of shells, of a given species have already been implicitly accounted for in the smoothing spline calculation. Of interest here are the causes of variability in the disequilibrium of calcium carbonate through time.

In planktonic formanifiera, recorded $\delta^{13}C$ is a strong function of shell size (e.g. Berger et al., 1978; Spero and Lea, 1993; Elderfield et al., 2002), and the difference in $\delta^{13}C$ between the largest and smallest size fractions can be greater than glacial-interglacial differences of the order of 0.5‰ (Oppo and Fairbanks, 1989). Therefore, $\delta^{13}C$ measurements from both planktonic and benthic species are usually made on shells selected for size fraction. Nevertheless, any unrecorded changes in shell size throughout a record may lead to significant error in $\Delta_{LGM}\delta^{13}C$. A second source of error is temperature-dependent fractionation, which affects planktonic species due to variability in surface temperature on seasonal to glacial timescales. The temperature-dependence of fractionation is a function of species. Culture experiment estimates of $\partial(\delta^{13}C)/\partial(T)$ (where T is temperature) have been made of -0.11‰ °C^{-1} for *Globigerina bulloides* (Bemis et al., 2000), -0.08‰ °C^{-1} for *Limacina inflata* (Fischer et al., 1999), 0 to $+0.05$‰ °C^{-1} for *Orbulina universa* (Bemis et al., 2000). No relationship with temperature was observed on *Globigerinoides ruber* (Fischer et al., 1999), whereas Kohfeld et al. (2000) assumed a relationship of -0.13‰ °C^{-1} for *Neogloboquadrina pachyderma*.

Culture experiments on planktonic foraminifera also reveal a strong dependence on the concentration of the carbonate ion, with a gradient of approximately -0.012‰/(μmol kg^{-1}) for *G. bulloides* under constant DIC. Glacial carbonate concentration is dependent on the poorly constrained alkalinity inventory of the ocean, but a change of 30 to 80 μmol kg^{-1} is not implausible (Kohfeld et al., 2000), indicating an effect of the same order as glacial $\delta^{13}C$ cycles. The effect of carbonate ion on benthic $\delta^{13}C$ is not known. A final effect arises due to changes in the isotopic composition of carbon in the diet; culture experiments indicate that $\delta^{13}C$ in *G. bulloides* shell carbonate varies as $\delta^{13}C$ in organic matter in the ratio 0.084:1 (Spero and Lea, 1996).

With the exception of sea-surface temperature reconstructions for the LGM (e.g. MARGO Project Members, 2009), variability in water properties likely to cause systematic errors in $\Delta_{LGM}\delta^{13}C$ are poorly constrained over the last 150 kyr, so no time-varying correction is applied to $\Delta_{LGM}\delta^{13}C$. Therefore, we caution that changes in these properties over a glacial cycle, rather than changes in seawater $\delta^{13}C$, may contribute significantly to variability in the the planktonic $\Delta_{LGM}\delta^{13}C$ record. However, Earth system models that output $\delta^{13}C$ can also produce temperature, alkalinity and pH fields, so that this is not an obstacle to model-data comparison; the validity of such comparisons are instead limited by the general applicability of the above empirical relationships. Moreover, we note that these caveats are a much lesser concern when interpreting the benthic δ^{13}C record.

A random error estimate may be made by comparing records from different species but from the same core. Among benthic species, the epibenthic taxon *Cibicidoides wuellerstorfi* is widely preferred for recording δ^{13}C, and to this species we ascribe an error, $2\sigma_{sp}$, of 0.15‰. This value is obtained from comparison of water column data (Kroopnick, 1985) with data from core samples (c.f. Beveridge et al., 1995). Error estimates for other species in the *Cibicidoides* genus were obtained using cores containing both *C. wuellerstorfi* and another *Cibicidoides* species. The error is the root-mean-squared (rms) difference between the two species after the application of an optimal species offset. This process was repeated for the infaunal genus *Uvigerina*. For other species, there was insufficient overlap in data with *C. wuellerstorfi* to apply this method. For these species, errors of 0.4‰ were ascribed. A larger error of 0.6‰ was applied to data derived from *Hoeglandia elegans* or from mixed benthics. Error estimates are presented in Table 2.

For planktonic foraminifera, the choice of reference species is less clear. We select *G. ruber*, which yields data that are consistent on a regional scale, and has a restricted depth range (Fischer et al., 1999), so that changes in recorded δ^{13}C are more likely to reflect changes in surface conditions. We ascribe an error of 0.4‰ to this species, and calculated estimates for *G. bulloides*, *Globigerinoides sacculifer*, and *N. pachyderma* by the same method used for benthic species. However, since these relative errors are less than 0.4‰, we ascribe an error of 0.4‰ to each of these species. These are presented in Table 2. We ascribe an error of 0.6‰ to other planktonic species.

3.2 Obtaining absolute δ^{13}C values

Absolute δ^{13}C values within each time-series are the sum of $\Delta_{LGM}\delta^{13}$C estimates and the LGM δ^{13}C value. The LGM δ^{13}C estimate is the value output from spline smoothing, plus any phytodetritus correction, plus a species-specific uniform correction. For the benthic genus *Cibicidoides* and the planktonic species *G. ruber*, we ascribe a correction of 0±0.2‰. The correction and correction error for other species are obtained by calculating the mean and standard deviation of the offsets used to optimise the least-squares-fit between different species in the same core, as described in Sect. 3.1.3. This precludes any spatial variability in the species offset, because despite evidence that these offsets change over a glacial cycle (Hoogakker et al., 2009b), there are insufficient data to quantify this variability globally. We obtain a correction of +0.85±0.48‰ for *Uvigerina* species, similar to the canonical value of +0.9‰ (Shackleton and Hall, 1984). Other estimates are given in Table 2; where no correction is quoted, no absolute δ^{13}C estimate is made.

4 δ^{13}C data presentation and interpretation

Data were separated into the principal regions: North Atlantic, South Atlantic, Indian Ocean and Pacific Ocean (Table 1), with subcategories for regions such as the Arctic Ocean, the Nordic Seas, and the South China Sea, and the Southern Ocean sector of each ocean, for which a highly inclusive definition of south of 40° S is used. By compiling all available δ^{13}C data in each region, presented as an anomaly relative to the LGM, and plotting on a uniform timescale, we can look for large scale changes in δ^{13}C that might be obscured or biased by consideration of a small number of cores. Nevertheless, there are sampling biases towards coastal areas in each ocean, towards the eastern Atlantic and towards the Arabian Sea in the Indian Ocean (Fig. 1), as well as towards the 2500–3500 m depth range. Data coverage is insufficient to interpolate and extrapolate in three dimensions, but estimates might be refined with new data or by dynamical smoothing using an Earth system model.

4.1 Benthic time-series

In Fig. 5 we present $\Delta_{LGM}\delta^{13}$C time-series grouped by region, excluding all data from the Arctic Ocean or from marginal seas (except the South China Sea), and by depth.

Only where the temporal resolution of the pre-processed data was sufficiently high (Δt<6 kyr) and the estimated error sufficiently low (<0.8‰) are data plotted. The mean and standard deviation, weighted by estimated error, of data from each region were calculated and are plotted in Fig. 6. Sampling biases towards coastal regions with high sedimentation rates are not removed in the averaging calculation. Therefore Fig. 6 is a representation of the range of data observed within each region, and not an unbiased estimate of regional averages.

In waters deeper than 2500 m, a consistent pattern is observed within the North Atlantic, South Atlantic, and Pacific Oceans. These basins exhibit maxima in δ^{13}C during temperature maxima, with small differences between the Eemian interglacial (MIS5e), the MIS5c and MIS5a interstadials, and the Holocene (MIS1). MIS4 and MIS6 are marked by values of δ^{13}C similar to or lower than LGM values, consistent with a longer timescale trend towards higher δ^{13}C (Hoogakker et al., 2006). The principal difference between the basins is in the amplitude of δ^{13}C variations. The North Atlantic exhibits slightly larger amplitude changes in δ^{13}C than the South Atlantic. The amplitude of the glacial cycle in the Pacific basin is approximately half that in the Atlantic basin. Furthermore, there is much less variability observed in the Pacific at around precessional timescales; MIS3 is a much weaker peak, whereas troughs during MIS5b and MIS5d are not consistently recorded. Typically lower sedimentation rates in the Pacific, leading to poorer data resolution, may contribute to the latter result. Another bias may arise from a weak positive correlation between bathymetric depth and the amplitude of variability. However, the mean depth of >2500 m cores in the Pacific (3400 m) is only slightly shallower than that in the Atlantic (3600 m), so this can explain less than 0.05‰ of the difference between the two basins. The lack of long records from deeper than 2500 m in the Indian Ocean prevent us from concluding whether there is similar variability in δ^{13}C over a full glacial cycle, although the amplitude of change between the LGM and the Holocene is greater than typical Pacific but lower than typical Atlantic amplitudes.

Much of the variability in deep $\Delta_{LGM}\delta^{13}$C is likely to arise from changes in the global ocean $\delta^{13}C$ reservoir, influenced by the storage of isotopically light carbon in the biosphere. This is supported by the qualitative similarity between the Pacific and the Atlantic $\Delta_{LGM}\delta^{13}C$, unless there are changes of the opposite sign within intermediate or pycnocline waters. There is some evidence, from Pacific cores in the 1500–2500 m depth range, for such changes over the time interval since the LGM (c.f. Duplessy et al., 1988b). However, records from a similar depth in the Indian Ocean, as well as shallower Pacific records, present a pattern that is broadly consistent with that observed in the deep Pacific.

Glacial variations in intermediate and pycnocline Atlantic $\delta^{13}C$ are thought to be strongly influenced by changes in the depth and range of the Atlantic overturning cell, in competition with Antarctic Bottom Water and Antarctic Intermediate Water, although changes in the partitioning of remineralised carbon have also been invoked (Boyle, 1988). Here, we note that Atlantic $\Delta_{LGM}\delta^{13}C$ in the 1500–2500 m depth range is similar to that observed in the Indian Ocean at the same depth, and in the deep Pacific Ocean. An exception is during deglaciations, when there are lower values of Atlantic intermediate water $\Delta_{LGM}\delta^{13}C$. Holocene $\Delta_{LGM}\delta^{13}C$ in <1500 m deep cores is usually negative, particularly in the West Atlantic, whereas there is no consistent pattern prior to the LGM.

4.2 Planktonic time-series and planktonic/benthic differences

Planktonic $\Delta_{LGM}\delta^{13}C$ time-series, grouped by region, are presented in Fig. 7. There is less agreement between different planktonic records within a region, compared to benthic records, consistent with the large uncertainty attributed to the estimation of seawater $\Delta_{LGM}\delta^{13}C$ from planktonic species (Sect. 3.1.3). *G. ruber* records from the North Atlantic and Indian Oceans consistently show elevated Holocene $\Delta_{LGM}\delta^{13}C$ values. Temperature maxima also exhibit higher $\Delta_{LGM}\delta^{13}C$ values than temperature minima in most *G. bulloides* records, although these changes are rarely outside the formal uncertainty limits. Notable exceptions are three cores from the Pacific sector of the

Southern Ocean, in which low early Holocene $\Delta_{LGM}\delta^{13}C$ values are recorded, and Indian Ocean cores, which exhibit little coherent variability over 150 000 yr, except for a slight upward trend. A decrease in $\Delta_{LGM}\delta^{13}C$ during MIS4 is present in most Atlantic records but less apparent in Pacific records. There is no clear evidence for minima in planktonic $\Delta_{LGM}\delta^{13}C$ during MIS5b and MIS5d, in contrast to benthic records from the deep Atlantic Ocean.

The difference between $\delta^{13}C$ recorded in planktonic and benthic foraminifera has long been of interest to paleooceanographers because of its association with deep ocean carbon storage (Broecker, 1982a; Shackleton et al., 1983), although interpreting changes in seawater $\delta^{13}C$ from planktonic data is problematic (Sect. 3.1.3). The difference between planktonic and benthic $\Delta_{LGM}\delta^{13}C$, $\Delta_{LGM}\delta^{13}C_{p-b}$, was calculated for each core with both planktonic and benthic $\delta^{13}C$ records. The weighted mean and standard deviation were calculated, at a regional scale, and are plotted in Fig. 8 (analogous to Fig. 6). There are few benthic/planktonic pairs from the Indian Ocean, or from shallower than 2500 m in the Pacific Ocean, so that averages are constructed from 3–8 benthic/planktonic pairs in each of these regions (averages are not constructed from fewer than three pairs). Throughout all regions, $\Delta_{LGM}\delta^{13}C_{p-b}$ remains within one standard deviation of zero for most of the 150 kyr record. The most notable features occur during deglaciations (MIS1/2 boundary; MIS5e/6 boundary), where $\Delta_{LGM}\delta^{13}C_{p-b}$ is usually negative outside the North Atlantic. The very low $\Delta_{LGM}\delta^{13}C_{p-b}$ values obtained for MIS1 in the Pacific are caused by anomalously low planktonic $\Delta_{LGM}\delta^{13}C$ in the Southern Ocean (Fig. 7); exclusion of these cores removes this feature.

Changes in the difference in $\delta^{13}C$ between surface and deep waters could be caused by changes in the relative strength of export production and meridional overturning in the global ocean. This is because the positive vertical $\delta^{13}C$ gradient, set up by the downward flux of isotopically light organic matter, is eroded by the exchange of upper ocean and deep waters. The weak $\delta^{13}C$ gradient found during deglaciations (i.e. the low value of $\Delta_{LGM}\delta^{13}C_{p-b}$) may indicate a decrease in export production, more rapid mixing between the deep and surface ocean, or a shift in downwelling towards isotopically heavier parts of the surface ocean. However, several other mechanisms influence $\Delta_{LGM}\delta^{13}C_{p-b}$, such as regional variability in productivity, circulation, and air-sea gas exchange, and periods of rapid growth or decline of the biosphere. It is also possible that variability in the $\Delta_{LGM}\delta^{13}C_{p-b}$ is dominated by variability in isotope disequilibria in planktonic foraminifera due to changes in temperature, diet, or carbonate ion concentration (Kohfeld et al., 2000).

4.3 Time slices and the role of ocean circulation in δ^{13}C change

A set of $\Delta_{LGM}\delta^{13}C$ time-slices for the Holocene (7 ka), MIS3 (49 ka), MIS5a (81 ka), MIS5b (87 ka) and MIS5e (123 ka) are plotted in Figs. 10–14. These are referenced to an absolute δ^{13}C time-slice for the LGM (21 ka), plotted in Fig. 9. We begin by describing the LGM state with reference to previous studies yielding LGM time-slices (e.g. Bickert and Mackensen, 2003; Curry and Oppo, 2005). Note that no uniform adjustment, representing changes in biosphere carbon storage (Duplessy et al., 1988b), is added to the time-slice. Horizontal gradients in deep (>2500 m) δ^{13}C are weaker than in modern observations (Kroopnick, 1985), with similar or lower values in the Atlantic Ocean than the Pacific Ocean. Isotopically light ($\delta^{13}C<0.5$ ‰) bottom waters penetrate north as far as the Iceland Basin, consistent with an expanded Antarctic overturning cell in the Atlantic Ocean relative to today. However, there persists a meridional gradient with isotopically heavier water in the north, consistent with an influence of North Atlantic source waters. At shallower depths, high δ^{13}C values are observed in the North Atlantic Ocean, increasing to ∼1.5 ‰ around 1000 m depth. This is consistent with the presence of an Atlantic source water, isotopically enriched relative to modern North Atlantic Deep Water, at depths currently occupied by Antarctic intermediate water (Curry and Oppo, 2005). In other basins, the available evidence is consistent with a weaker vertical δ^{13}C gradient than that found in the Atlantic, with no minimum at ∼2000 m such as is observed in the modern ocean (c.f. Duplessy et al., 1988b).

Whereas the present study is concerned with the global δ^{13}C record over a glacial cycle, Bickert and Mackensen (2003) and Curry and Oppo (2005) focused on compiling benthic LGM time-slices for the Atlantic ocean. These studies include cores, mostly from the West Atlantic, that are absent from our synthesis due to the age modelling constraint (Sect. 2.1). These cores reveal a zonal gradient in the LGM South Atlantic at intermediate depths, with isotopically lighter water of southern origin in the west (Curry and Oppo, 2005), and isotopically heavier water of possible Mediterranean origin near the eastern boundary (Bickert and Mackensen, 2003). Our time-slice also excludes data from the Matsumoto and Lynch-Stieglitz (1999) compilation of southeast Pacific LGM data, where individual foraminer shells were interpreted as representing the LGM, based on $\delta^{18}O$ measurements. They obtained glacial $\delta^{13}C$ estimates of between −0.35 and −0.6‰ in the 2800–3800 m depth range.

The Holocene time-slice (Fig. 10) exhibits deep Atlantic $\Delta_{LGM}\delta^{13}C$ values that are 0.4–1.0‰ higher than LGM values, with lower but positive $\Delta_{LGM}\delta^{13}C$ in the Indian and Pacific oceans. The Atlantic values are likely to be the sum of an ocean reservoir effect and changes in oceanic processes in the Atlantic Ocean. In the South Atlantic, the anomalously high Holocene $\Delta_{LGM}\delta^{13}C$ is attributed to an increase in $\delta^{13}C$ of the southern end member (Curry and Oppo, 2005). This could be caused by more rapid air-sea gas exchange in the Southern Ocean or by changes in ventilation rates of the Southern Ocean (Marchitto and Broecker, 2006; Toggweiler et al., 2006). Further north, changes in the end member and the expansion of North Atlantic source water both contribute to high values of $\Delta_{LGM}\delta^{13}C$. Lower values of $\Delta_{LGM}\delta^{13}C$ are observed at shallower depths throughout the global ocean, where observations exist, including negative values at <1500 m in the Atlantic Ocean. Low latitude planktonic $\Delta_{LGM}\delta^{13}C$ is typically similar to that observed in the deep ocean, although there is much greater scatter in the data. Negative or near-zero values of planktonic $\Delta_{LGM}\delta^{13}C$ occur to the south of the Greenland-Scotland Ridge, along with positive values in the Nordic seas, and are consistent with a northward shift in deep ocean ventilation between the LGM and the Holocene (Labeyrie and Duplessy, 1985).

The 49 ka time-slice (Fig. 11) represents the maximum in deep ocean $\Delta_{LGM}\delta^{13}C$

during MIS3 (Fig. 6). As with the 7 ka time-slice, positive deep $\Delta_{LGM}\delta^{13}C$ and negative or near-zero $\Delta_{LGM}\delta^{13}C$ at intermediate depths are observed in the Atlantic Ocean, though the changes are of much smaller amplitude. However, deep $\Delta_{LGM}\delta^{13}C$ in the Southern Ocean is negative or near-zero. Moreover, bottom waters in the low latitude South Atlantic exhibit smaller increases in $\Delta_{LGM}\delta^{13}C$ than waters at ~3000 m depth (not shown). To the extent that Holocene data are consistent with an expansion of Atlantic source waters and an increase in southern end-member $\delta^{13}C$, MIS3 data are consistent with an expansion of Atlantic source waters (relative to the LGM) and a decrease in southern end-member $\delta^{13}C$. An MIS4 timeslice is presented only in the Supplementary Materials (http://www.clim-past-discuss.net/5/2497/2009/cpd-5-2497-2009-supplement.zip) because no clear pattern of change relative to MIS2 is obtained; there are generally higher values of $\Delta_{LGM}\delta^{13}C$ in the North Atlantic than the South Atlantic, but this gradient is small compared with the uncertainty in the data.

The 81 ka time-slice (Fig. 12) occurs during MIS5a, the final maximum in $\Delta_{LGM}\delta^{13}C$ before dropping to low values that persist from MIS4 to MIS2. Comparison of Figs. 12 and 14 reveals that only the Southern Ocean exhibits consistently lower $\Delta_{LGM}\delta^{13}C$ during MIS5a then MIS5e, nor is there a change in the gradient between intermediate and deep $\Delta_{LGM}\delta^{13}C$. This is despite much of the glacial decrease in atmospheric pCO_2 and most of the decrease in Antarctic temperature occurring between MIS5e and MIS5a, rather than between MIS5a and MIS4 (Fig. 6). Planktonic $\Delta_{LGM}\delta^{13}C$ in much of the ocean is higher during MIS5a than MIS5e, however. The 87 ka time-slice (Fig. 13) occurs during MIS5b, a local minimum in deep Atlantic $\Delta_{LGM}\delta^{13}C$ within the generally high values observed during MIS5. A pattern is observed that is more similar to MIS3 than the Holocene, with lower values of $\Delta_{LGM}\delta^{13}C$ in the Southern Ocean than elsewhere in the deep ocean (albeit higher than in MIS3). This is consistent with the findings of Govin et al. (2009) that the decrease in Southern Ocean $\delta^{13}C$ occurs early during glacial inception, predating changes in the North Atlantic.

The 123 ka time-slice (Fig. 14) represents the last interglacial (MIS5e), and resembles the Holocene time-slices where data are available. The greatest discrepancy is that lower values of planktonic $\Delta_{LGM}\delta^{13}C$ are found in the low latitude Atlantic Ocean during MIS5e. Globally, $\Delta_{LGM}\delta^{13}C$ values are lower by 0–0.1 ‰. An MIS6 timeslice is presented only in the Supplementary Materials (http://www.clim-past-discuss.net/5/2497/2009/cpd-5-2497-2009-supplement.zip), because it is indistinguishable from MIS2, except for globally lower values during MIS6 by 0.1–0.2 ‰.

5 Discussion

We have presented benthic and planktonic $\delta^{13}C$ data over the last 150 kyr. The reasonable global coverage within the synthesis depends on the inclusion of records from a variety of species, from high-productivity regions, and from regions with low sedimentation rates. This approach makes uncertainties an essential part of the data set; these were obtained using the entire dataset to estimate the additional error present in data from low resolution records and in less reliable species. Errors are smaller for estimates of $\Delta_{LGM}\delta^{13}C$, the anomaly relative to the local LGM value, than for the absolute $\delta^{13}C$ because a large component of error is uniform within each record. $\Delta_{LGM}\delta^{13}C$ timeslices have the advantage over $\delta^{13}C$ timeslices as a modelling target that the latter target may favour states with errors that compensate for model error in the Holocene $\delta^{13}C$ distribution. We caution that, due to imprecision in the age-models, the data synthesis should not be used to examine inter-basin differences on timescales shorter than 6 kyr. A final caveat is that much remains to be learnt about how foraminifera record changes in properties other than seawater $\delta^{13}C$. Several such properties (notably temperature, pCO_2 and carbonate ion concentration) are likely to change over a glacial cycle and introduce systematic errors to $\delta^{13}C$ change estimates (Sect. 3.1.3). This is of particular importance for data from planktonic foraminifera. We therefore caution that recorded variability in planktonic $\delta^{13}C$ may result from changes in ocean temperature and chemistry rather than in seawater $\delta^{13}C$.

The data synthesis reveals a high degree of spatial coherence in $\delta^{13}C$ variability in the deep Atlantic and Pacific Oceans, with high values during temperature maxima and low values during temperature minima. The amplitude of variability in the Atlantic Ocean is approximately double that in the Pacific, suggesting that the δ^{13}C reservoir effect and ocean processes influencing deep Atlantic δ^{13}C act in phase and are of similar magnitude. The relative lack of variability in intermediate-depth North Atlantic δ^{13}C is consistent with a shoaling of ^{13}C rich North Atlantic source waters during cold periods. The available data from outside the Atlantic Ocean also show less variability at intermediate depths. Atlantic δ^{13}C appears to be influenced by increases in δ^{13}C of the southern end-member during interglacials, but not during other temperature maxima. There is little evidence for basin-scale differences in δ^{13}C between MIS1, 5a, 5c and 5e, or between MIS2, 4 and 6 (except for the globally lower δ^{13}C values obtained during MIS 6), although individual records may show such differences. δ^{13}C at a given location may be interpreted in terms of highly local processes rather than large scale processes discusses in this paper. We therefore recommend that care be taken when using small numbers of records to infer changes in global phenomena. The similarity between MIS 5a and 5e suggests that the relationship between δ^{13}C and atmospheric pCO_2 over glacial cycles is complex. The major change in the δ^{13}C record occurs between MIS 5a and MIS 4, whereas much of the decrease in pCO_2 (and almost all of the decrease in Antarctic temperature) occurs between MIS 5e and MIS 5a (Fig. 6). Therefore, either the drawdown of pCO_2 during early glaciation occurred by a mechanism that does not decrease deep ocean δ^{13}C or there was a compensating mechanism acting to increase deep ocean δ^{13}C without increasing pCO_2.

Constructing δ^{13}C inventories would be a valuable tool in estimating changes in carbon storage in the terrestrial biosphere and shelf sediments. Duplessy et al. (1988b) used Pacific data only to estimate the increase in ocean mean δ^{13}C between the LGM and the Holocene as +0.32‰, yielding a smaller change in carbon storage than is suggested by paleoecological reconstructions (Crowley, 1995; Peng et al., 1998). Despite the coherence of the data, we consider the coverage too incomplete to directly construct a time-series of δ^{13}C inventories. The principal gaps in benthic data suited to our age modelling method are in the Indian Ocean, intermediate depths in the Pacific Ocean, the Southern Ocean, and pycnocline depths throughout the global ocean. Nevertheless, there are sufficient data to tightly constrain the evolution of an Earth system model, and we propose data assimilation into such a model as a viable means to reconstruct biosphere carbon storage over the last glacial cycle.

Acknowledgements. This study was funded by the NERC Quaternary QUEST programme. K. Oliver was supported by a Leverhulme Early Career Research Fellowship. We are grateful to the many researchers who have assisted us in compiling the data either through personal correspondence or by making records available via Pangaea or NGDC, and for data obtained through the DELPHI project.

References

Abrantes, F., Baas, J., Haflidason, H., Rasmussen, T. L., Klitgaard, D., Loncaric, N., and Gaspar, L.: Sediment fluxes along the northeastern European Margin: inferring hydrological changes between 20 and 8 kyr, Mar. Geol., 152, 7–23, 1998. 2539

Anderson, D. M., Prell, W. L., and Barratt, N. J.: Estimates of sea surface temperature in the Coral Sea at the last glacial maximum, Paleoceanography, 4, 615–627, 1989. 2539

Arz, H. W., Pätzold, J., and Wefer, G.: The deglacial history of the western tropical Atlantic as inferred from high resolution stable isotope records off northeastern Brazil, Earth Planet. Sci. Lett., 167, 105–117, 1999. 2539

Bassinot, F. C., Beaufort, L., Vincent, E., Labeyrie, L., Rostek, F., Müller, P. J., Quidelleur, X., and Lancelot, Y.: Coarse fraction fluctuations in pelagic carbonate sediments from the tropical Indian Ocean: A 1500-kyr record of carbonate dissolution, Paleoceanography, 9, 579–600, 1994. 2539

Bauch, H., Erlenkeuser, H., Spielhagen, R. F., Struck, U., Matthiessen, J., Thiede, J., and Heinemeier, J.: A multiproxy reconstruction of the evolution of deep and surface waters in the subarctic Nordic seas over the last 30 000 years, Quat. Sci. Rev., 20, 659–678, 2001. 2539

Bemis, B. E., Spero, H. J., Lea, D. W., and Bijma, J.: Temperature influence on the carbon

CPD

5, 2497–2554, 2009

Synthesis of marine $\delta^{13}C$

K. I. C. Oliver et al.

Title Page

Abstract | Introduction

Conclusions | References

Tables | Figures

◀| |▶

◀ ▶

Back | Close

Full Screen / Esc

Printer-friendly Version

Interactive Discussion

isotopic composition of *Globigerina bulloides* and *Orbulina universa* (planktonic foraminifera), Mar. Micropaleontol., 38, 213–228, 2000. 2509
Berger, W. H., Killingley, J. S., and Vincent, E.: Stable isotopes in deep-sea carbonates: box core ERDC-92 west equatorial Pacific, Oceanol. Acta, 1, 203–216, 1978. 2508
Beveridge, N. A. S., Elderfield, H., and Shackleton, N. J.: Deep thermohaline circulation in the low-latitude Atlantic during the last glacial, Paleoceanography, 10, 643–660, 1995. 2510, 2539
Bickert, T. and Mackensen, A.: Last Glacial to Holocene Changes in South Atlantic deep water circulation, in: The South Atlantic in the late Quaternary: Reconstruction of material budgets and current systems, edited by: Wefer, G., Mulitza, S., and Ratmeyer, V., 671–695, Springer-Verlag, Berlin Heidelberg New York Tokyo, 2003. 2500, 2504, 2507, 2515, 2516, 2539
Bickert, T. and Wefer, G.: Late Quaternary deep water circulation in the South Atlantic: Reconstruction from carbonate dissolution and benthic stable isotopes, in: The South Atlantic in the late Quaternary: Present and Past Circulation, edited by: Wefer, G., Berger, W. H., Siedler, G., and Webb, D., 599–620, 1996. 2539
Bickert, T. and Wefer, G.: South Atlantic and benthic foraminifer δ^{13}C-deviations: Implications for reconstructing the Late Quaternary deep-water circulation, Deep-Sea Res. I, 46, 437–452, 1999. 2507
Bickert, T., Curry, W. B., and Wefer, G.: Late Pliocene to Holocene (2.60 Ma) western equatorial Atlantic deep-water circulation: Inferences from stable isotopes, Proc. Ocean Drill. Program Sci. Results, 154, 239–253, 1997. 2539
Boyle, E.: Vertical oceanic nutrient fractionation and glacial/interglacial CO_2 cycles, Nature, 331, 55–56, 1988. 2513
Broecker, W. S.: Ocean chemistry during glacial time, Geochem. Cosmochim. Acta, 46, 1689–1705, 1982a. 2499, 2514
Broecker, W. S.: Tracers in the Sea, Eldigio Press, New York, 690 pp., 1982b. 2499
Brovkin, V., Ganapolski, A., Archer, D., and Rahmstorf, S.: Lowering of glacial atmospheric CO_2 in response to changes in oceanic circulation and marine biogeochemistry, Paleoceanography, 22, PA4202, doi:10.1029/2006PA001380, 2007. 2499
Cannariato, K. G. and Ravelo, A. C.: Pliocene-Pleistocene evolution of eastern tropical Pacific surface water circulation and thermocline depth, Paleoceanography, 12, 805–820, 1997. 2539
Carter, L., Manighetti, B., Ganssen, G., and Northcote, L.: Southwest Pacific modulation of

abrupt climate change during the Antarctic Cold Reversal Younger Dryas, Palaeogeogr. Palaeoclimatol. Palaeoecol., 260, 284–298, 2008. 2539

Chapman, M. R. and Shackleton, N. J.: Global ice-volume fluctuations, North Atlantic ice-rafting events, and deep-ocean circulation changes between 130 and 70 ka, Geology, 27, 795–798, 1999. 2539

Cortijo, E.: Stable isotope analysis on sediment core SU90-39, PANGAEA, doi:10.1594/PANGAEA.106761, 2003. 2539

Crowley, T. J.: Ice age terrestrial carbon changes revisited, Glob. Biogeochem. Cyc., 9, 377–389, 1995. 2519

Curry, W. B. and Oppo, D. W.: Synchronous, high-frequency oscillations in tropical sea surface temperatures and North Atlantic Deep Water productivity during the last glacial cycle, Paleoceanography, 12, 1–14, 1997. 2539

Curry, W. B. and Oppo, D. W.: Glacial water mass geometry and the distribution of $\delta^{13}C$ of ΣCO_2 in the western Atlantic Ocean, Paleoceanography, 20, PA1017, doi:10.1029/2004PA001021, 2005. 2500, 2515, 2516, 2539

Curry, W. B., Duplessy, J.-C., Labeyrie, L., and Shackleton, N. J.: Changes in the distribution of $\delta^{13}C$ of deep water ΣCO_2 between the last glaciation and the Holocene, Paleoceanography, 3, 317–341, 1988. 2539

Dorschel, B., Hebbeln, D., Rüggeberg, A., Dullo, W.-C., and Freiwald, A.: Growth and Erosion of a Cold-Water Coral Covered Carbonate Mound in the Northeast Atlantic during the Late Pleistocene and Holocene, Earth and Planet. Sci. Lett., 233, 33–44, 2005. 2539

Duplessy, J.-C.: Quaternary paleoceanography: unpublished stable isotope records. IGBP PAGES/World Data Center for Paleoclimatology Data Contribution Series #1996-035., NOAA/NGDC Paleoclimatology Program, Boulder, Colorado, USA, 1996. 2539

Duplessy, J. C., Bé, A. W. H., and Blanc, P. L.: Oxygen and carbon isotopic composition and biogeographic distribution of planktonic foraminifera in the Indian Ocean, Palaeogeogr. Palaeoclimatol. Palaeoecol., 33, 9–46, 1981. 2499

Duplessy, J. C., Labeyrie, L., and Blanc, P. L.: Norwegian Sea Deep Water variations over the last climatic cycle: Paleo-oceanographical implications, in: Long and Short Term Variability of Climate, edited by: Wanner, H. and Siegenthaler, U., 83–116, Springer, Heidelberg, 1988a. 2539

Duplessy, J. C., Shackleton, N. J., Fairbanks, R. G., Labeyrie, L., Oppo, D., and Kallel, N.: Deepwater source variations during the last climatic cycle and their impact on the global

CPD

5, 2497–2554, 2009

deepwater circulation, Paleoceanography, 3, 343–360, 1988b. 2499, 2513, 2515, 2519
Duplessy, J.-C., Labeyrie, L., Arnold, M., Paterne, M., Duprat, J., and van Weering, T. C. E.: Changes of surface salinity of the North Atlantic ocean during the last deglaciation, Nature, 358, 485–488, 1992. 2539
Dürkop, A., Hale, W., Mulitza, S., Pätzold, J., and Wefer, G.: Late Quaternary variations of sea surface salinity and temperature in the western tropical Atlantic: Evidence from δ^{18}O of Globigerinoides sacculifer, Paleoceanography, 12, 764–772, 1997. 2539
Elderfield, H., Vautravers, M., and Cooper, M.: The relationship between shell size and Mg/Ca, Sr/Ca, δ^{18}O and δ^{13}C of species of planktonic foraminifera, Geochem. Geophys. Geosyst., 3, 2001GC000194, 2002. 2508
Enting, I.: On the use of smoothing splines to filter CO_2 data, J. Geophys. Res., 92, 10 977–10 984, 1987. 2505
EPICA community members: Eight glacial cycles from an Antarctic ice core, Nature, 429, 623–628, doi:10.1038/nature02599, 2004. 2546, 2548
Fischer, G. and Wefer, G. (Eds.): Use of Proxies in Paleoceanography: Examples from the South Atlantic, Springer-Verlag, Berlin Heidelberg New York Tokyo, 1999.
Fischer, G., Kalberer, M., Donner, B., and Wefer, G.: Stable isotopes of pteropod shells as recorders of sub-surface water conditions: Comparison to the record of *G. ruber* and to measured values, in: Use of Proxies in Paleoceanography: Examples from the South Atlantic, edited by: Fischer, G. and Wefer, G., 191–206, 1999. 2509, 2510
Freudenthal, T., Meggers, H., Henderiks, J., Kuhlmann, H., Moreno, A., and Wefer, G.: Upwelling intensity and filament activity off Morocco during the last 250 000 years, Deep Sea Res. II, 49, 3655–3674, 2002. 2539
Gorbarenko, S. A. and Southon, J. R.: Detailed Japan Sea paleoceanography during last 25 Kyr: constraints from AMS dating and δ^{18}O of planktonic foraminifera, Palaeogeogr. Palaeoclimatol. Palaeoecol., 156, 177–193, 2000. 2539
Govin, A., Michel, E., Labeyrie, L., Waelbroeck, C., Dewilde, F., and Jansen, E.: Evidence for northward expansion of Antarctic Bottom Water mass in the Southern Ocean during the last glacial inception, Paleoceanography, 14, PA1202, doi:10.1029/2008PA001603, 2009. 2517
Hale, W. and Pflaumann, U.: Sea-surface Temperature Estimations using a Modern Analog Technique with Foraminiferal Assemblages from Western Atlantic Quaternary Sediments, in: Use of Proxies in Paleoceanography: Examples from the South Atlantic, edited by: Fischer, G. and Wefer, G., 69–90, 1999. 2539

Hodell, D. A., Venz, K. A., Charles, C. D., and Ninnemann, U. S.: Pleistocene vertical carbon isotope and carbonate gradients in the South Atlantic sector of the Southern Ocean, Geochem. Geophy. Geosy., 4, doi:10.1029/2002GC000367, 2003. 2539

Holbourn, A. E., Kuhnt, W., and James, N.: Late Pleistocene bryozoan reef mounds of the Great Australian Bight: isotope stratigraphy and benthic foraminiferal record, Paleoceanography, 17, doi:10.1029/2001PA000 643, 2002. 2539

Hoogakker, B. A. A., Crowhurst, S. C., Oliver, K. I. C., and Elderfield, H.:: A synthesis of marine sediment core δ^{18}O data over the last 150 000 years, in prep. for Clim. Past, 2009a. 2500, 2501, 2502

Hoogakker, B. A. A., Elderfield, H., Oliver, K. I. C., and Crowhurst, S.: Benthic foraminiferal isotope offsets over the last glacial-interglacial cycle, submitted to Paleoceanography, 2009b. 2506, 2511

Hoogakker, B. A. A., Rohling, E. J., Palmer, M. R., Tyrrell, T., and Rothwell, R. G.: Underlying causes for long-term global ocean δ^{13}C fluctuations over the last 1.20 Myr, Earth Planet. Sci. Lett., 248, 15–29, 2006. 2512

Howard, W. R. and Prell, W. L.: Late Quaternary carbonate production and preservation in the Southern Ocean: implications for oceanic and atmospheric carbon cycling, Paleoceanography, 9, 453–482, 1994. 2539

Hüls, M.: Stable isotope analysis on sediment core M35003-4, PANGAEA, 29, doi:10.1594/PANGAEA.55754, 1999. 2539

Imbrie, J., McIntyre, A., and Mix, A. C.: Composite stable isotope data (adjusted) for sediment core RC12-294 (specmap.002), PANGAEA, doi:10.1594/PANGAEA.52117, 1997. 2539

Jung, S. J. A.: Stable isotope analysis of foraminifera from sediment core SO82_5-2, PANGAEA, doi:10.1594/PANGAEA.201812, 2004. 2539

Jung, S. J. A. and Sarnthein, M.: Stable isotope data of sediment cores GIK23419-8, PANGAEA, doi:10.1594/PANGAEA.112916, 2003a. 2539

Jung, S. J. A. and Sarnthein, M.: Stable isotope data of sediment cores GIK23414-9, PANGAEA, doi:10.1594/PANGAEA.112911, 2003b. 2539

Jung, S. J. A. and Sarnthein, M.: Stable isotope data of sediment cores GIK23415-9, PANGAEA, doi:10.1594/PANGAEA.112912, 2003c. 2539

Jung, S. J. A. and Sarnthein, M.: Stable isotope data of sediment cores GIK23418-8, PANGAEA, doi:10.1594/PANGAEA.112915, 2003d. 2539

Jung, S. J. A. and Sarnthein, M.: Stable isotope data of sediment cores GIK23417-1, PAN-

GAEA, doi:10.1594/PANGAEA.112914, 2003e. 2539

Jung, S. J. A. and Sarnthein, M.: Stable isotope analysis of foraminifera from sediment cores GIK17049-6, PANGAEA, doi:10.1594/PANGAEA.112908, 2004a. 2539

Jung, S. J. A. and Sarnthein, M.: Stable isotope data of core GIK23416-4, PANGAEA, doi:10.1594/PANGAEA.136423, 2004b. 2539

Jung, S. J. A., Kroon, D., Ganssen, G., Peeters, F., and Ganeshram, R.: Enhanced Arabian Sea intermediate water flow during glacial North Atlantic cold phases, Earth Planet. Sci. Lett., 280, 220–228, 2009. 2539

Kawamura, H., Holbourn, A. E., and Kuhnt, W.: Climate variability and land? Ocean interactions in the Indo Pacific Warm Pool: A 460-ka palynological and organic geochemical record from the Timor Sea, Mar. Micropaleontol., 59, 1–14, 2006. 2539

Keigwin, L. D.: Radiocarbon and stable isotope constraints on Last Glacial Maximum and Younger Dryas ventilation in the western North Atlantic, Paleoceanography, 19, PA4012, doi:10.1029/2004PA001029, 2004. 2539

Kohfeld, K. E., Anderson, R. F., and Lynch-Stieglitz, J.: Carbon isotopic disequilibrium in polar planktonic foraminifera and its impact on modern and Last Glacial Maximum reconstructions, Paleoceanography, 15, 53–64, 2000. 2509, 2515

Kroopnick, P.: The distribution of ^{13}C of TCO_2 in the world oceans, Deep Sea Res., 32, 57–84, 1985. 2510, 2515

Labeyrie, L.: Quaternary paleoceanography: unpublished stable isotope records. IGBP PAGES/World Data Center for Paleoclimatology Data Contribution Series #1996-036, NOAA/NGDC Paleoclimatology Program, Boulder, Colorado, USA, 1996. 2539

Labeyrie, L.: Stable isotope analysis on foraminifera from sediment core MD88-770, PANGAEA, doi:10.1594/PANGAEA.52728, 1998. 2539

Labeyrie, L., Vidal, L., Cortijo, E., Paterne, M., Arnold, M., Duplessy, J.-C., Vautravers, M., Labracherie, M., Duprat, J., Turon, J. L., Grousset, F., and Van Weering, T.: Surface and deep hydrology of the Northern Atlantic Ocean during the last 150 000 years, Phil. Trans. Royal Soc. London, B, 348, 255–264, 1995. 2539

Labeyrie, L. D. and Duplessy, J. C.: Changes in the oceanic $^{13}C/^{12}C$ ratio during the last 140 000 years: high-latitude surface water records, Palaeogeogr. Palaeoclimatol. Palaeoecol., 50, 217–240, 1985. 2516

Lea, D. W., Pak, D. K., and Spero, H. J.: Climate impact of late Quaternary, equatorial Pacific sea surface temperature variations, Science, 289, 1719–1724, 2000. 2539

Lowry, R. K., Machin, P., and Cramer, R. N.: BOFS North Atlantic Data Set. Oceanographic data collected during the North Atlantic cruises of the NERC Biogeochemical Ocean Flux Study (1989–1991): a UK contribution of JGOFS, Natural Environmental Research Council, British Oceanographic Data Centre, Merseyside, UK, 1994. 2539

Lynch-Stieglitz, J., Curry, W., and Oppo, D.: Meridional overturning circulation in the South Atlantic at the last glacial maximum, Geochem. Geophys. Geosyst., 7, doi:10.1029/2005GC001226, 2006. 2539

Lynch-Stieglitz, J., Adkins, J. F., Curry, W. B., Dokken, T., Hall, I. R., Herguera, J. C., Hirschi, J. J.-M., Ivanova, E., Kissell, C., Marchal, O., Marchitto, T. M., McCave, I. N., McManus, J. F., Mulitza, S., Ninnemann, U. S., Yu, E.-F., and Zahn, R.: Atlantic overturning circulation during the last glacial maximum, Science, 316, 66–69, 2007. 2500

Mackensen, A., Hubberten, H. W., Bickert, T., Fischer, G., and Fütterer, D. K.: δ^{13}C in benthic foraminiferal tests of *Fontbotia wuellerstorfi* (Schwager) relative to δ^{13}C of dissolved inorganic carbon in Southern Ocean deep water: implications for glacial ocean circulation models, Paleoceanography, 8, 587–610, 1993. 2507

Mackensen, A., Grobe, H., Hubberten, H. W., and Kuhn, G.: Benthic foraminiferal assemblages and the δ^{13}C-signal in the Atlantic sector of the Southern Ocean: Glacial-to-interglacial contrasts, in: Carbon Cycling in the Glacial Ocean: Constraints on the Ocean's Role in Global Change, edited by: Zahn, R., Kaminski, M., Labeyrie, L., and Pedersen, T., 105–144, NATO ASI series, Springer, Berlin, I 17, 1994. 2539

Mackensen, A., Rudolph, M., and Kuhn, G.: Late Pleistocene deep-water circulation in the subantarctic eastern Atlantic, Glob. Planet Change, 30, 197–229, 2001. 2508, 2539

Marchitto, T. M. and Broecker, W. S.: Deep water mass geometry in the glacial Atlantic Ocean: A review of constraints from the paleonutrient proxy Cd/Ca, Geochem. Geophys. Geosys., 7, 10.1029/2006GC001323, 2006. 2499, 2516

MARGO Project Members: Constraints on the magnitude and patterns of ocean cooling at the Last Glacial Maximum, Nature Geosci., 2, 127–132, 2009. 2509

Martinson, D. G., Pisias, N. G., Hays, J. D., Imbrie, J. D., Moore, T. C., and Shackleton, N. J.: Age Dating and the orbital theory of the ice ages: development of a high-resolution 0 to 300 000-year chronostratigraphy, Quaternary Res., 27, 1–29, 1987. 2539

Matsumoto, K. and Lynch-Stieglitz, J.: Similar glacial and Holocene deep water circulation inferred from southeast Pacific benthic foraminiferal carbon isotope composition, Paleoceanography, 14, 149–163, 1999. 2516

McCave, I. N., Carter, L., and Hall, I. R.: Glacial-interglacial changes in water mass structure and flow in the SW Pacific, Quaternay Sci. Rev., 27, 1886–1908, doi:10.1016/j.quascirev.2008.07.010, 2008. 2539

McConnaughey, T. A., Burdett, J., Whelan, J. F., and Paull, C. K.: Carbon isotopes in biological carbonates: respiration and photosynthesis, Geochim. Cosmochim. Acta, 62, 611–622, 1997. 2508

McIntyre, A., Ruddiman, W. F., Karlin, K., and Mix, A. C.: Surface water response of the Equatorial Atlantic Ocean to orbital forcing, Paleoceanography, 4, 19–55, 1989. 2539

Mix, A. C., Pisias, N. G., Zahn, R., Rugh, W., Lopez, C., and Nelson, K.: Carbon 13 in Pacific deep and intermediate waters, 0–370 ka: implications for ocean circulation and Pleistocene CO_2, Paleoceanography, 6, 205–226, 1991. 2539

Mollenhauer, G., Schneider, R. R., Müller, P. J., Spiess, V., and Wefer, G.: Glacial/interglacial variability in the Benguela upwelling system: Spatial distribution and budgets of organic carbon accumulation, Glob. Biogeochem. Cyc., 16, doi:10.1029/2001GB001488, 2002. 2539

Monnin, E., Indermuhle, A., Dallenbach, A., Fluckiger, J., Stauffer, B., Stocker, T. F., Raynard, D., and Barnola, J. M.: Atmospheric CO_2 concentrations over the last glacial termination, Science, 291, 112–114, 2001. 2546, 2548

Morley, J. J., Heusser, L. E., and Shackleton, N. J.: Late Pleistocene/Holocene radiolarian and pollen records from sediments in the sea of Okhotsk, Paleoceanography, 6, 121–131, 1991. 2539

Mulitza, S.: Stable isotopes of sediment core GeoB1523-2, PANGAEA, doi:10.1594/PANGAEA.54618, 1998. 2539

Nørgaard-Pedersen, N., Spielhagen, R. F., Thiede, J., and Kassens, H.: Central Arctic surface ocean environment during the past 80 000 years, Paleoceanography, 13, 193–204, 1998. 2539

Oppo, D. W. and Fairbanks, F. G.: Variability in the deep and intermediate water circulation of the Atlantic Ocean during the past 25 000 years: Northern Hemisphere modulation of the Southern Ocean, Earth Planet. Sci. Lett., 86, 1–15, 1987. 2539

Oppo, D. W. and Fairbanks, R. G.: Carbon isotopic comparison of tropical surface water during the past 22 000 year, Paleoceanography, 4, 333–351, 1989. 2508

Oppo, D. W. and Lehmann, S. J.: Suborbital timescale variability of North Atlantic Deep Water during the past 200 000 years, Paleoceanography, 10, 901–910, 1995. 2539

Oppo, D. W., Fairbanks, R. G., Gordon, A. L., and Shackleton, N. J.: Late Pleistocene Southern

Ocean δ^{13}C variability, Paleoceanography, 5, 43–54, 1990. 2539
Oppo, D. W., McManus, J. F., and Cullen, J. L.: Palaeo-oceanography: Deepwater variability in the Holocene epoch, Nature, 422, 277, 2003. 2539
Pahnke, K., Zahn, R., Elderfield, H., and Schulz, M.: 340 000-Year centennial-scale marine record of Southern Hemisphere climatic oscillation, Science, 301, 948–952, 2003. 2539
Patrick, A. and Thunell, R. C.: Tropical Pacific sea surface temperatures and upper water column thermal structure during the last glacial maximum, Paleoceanography, 12, 649–657, 1997. 2539
Paul, A. and Multiza, S.: Challenges to Understanding Ocean Circulation during the Last Glacial Maximum, Eos, 90, 167–167, 2009. 2504
Peng, C. H., Guiot, J., and Van Campo, E.: Estimating changes in terrestrial vegetation and carbon storage: using paleoecological data and models, Quat. Sci. Rev., 17, 719–735, 1998. 2519
Petit, J. R.: Climate and atmospheric history of the past 420 000 years from the Vostok ice core, Nature, 399, 429–436, 1999. 2546, 2548
Pierre, C., Saliege, J. F., Urrutiaguer, M. J., and Giraudeau, J.: Stable isotope record of the last 500 k.y. at Site 1087 (Southern Cape Basin), Proc. Ocean Drill. Program Sci. Results, 175, 2001. 2539
Prell, W. L., Hutson, W. H., Williams, D. F., Bé, A. W. H., Geitzenauer, K., and Molfino, B.: Surface circulation of the Indian Ocean during the last glacial maximum, approximately 18 000 yr B.P., Quaternary Res., 14, 309–336, 1980. 2539
Rau, A., Roger, J., Lutjeharms, J., Giraudeau, J., Lee-Thorp, J., Chen, M.-T., and Waelbroeck, C.: A 450-kyr record of hydrological conditions on the western Agulhas Bank Slope, south of Africa, Marine Geol., 180, 183–201, doi:10.1016/S0025–3227(01)00213–4, 2002. 2539
Richter, T.: Stable isotope data of sediment core GEOFAR KF09, PANGAEA, doi:10.1594/PANGAEA.66316, 2001. 2539
Rickaby, R. E. M. and Elderfield, H.: Planktonic foraminiferal Cd/Ca: Paleonutrients or paleotemperature?, Paleoceanography, 14, 293–303, 1999. 2539
Rickaby, R. E. M., Elderfield, H., Roberts, N., Hillenbrand, C.-D., and Mackensen, A.: Evidence for elevated alkalinity in the glacial Southern Ocean, Paleoceanography, doi:10.1029/2009PA001762, in press, 2009. 2539
Ridgwell, A., Hargreaves, J. C., Edwards, N. R., Annan, J. D., Lenton, T. M., Marsh, R., Yool, A., and Watson, A.: Marine geochemical data assimilation in an efficient Earth System Model of

global biogeochemical cycling, Biogeosciences, 4, 87–104, 2007, http://www.biogeosciences.net/4/87/2007/. 2499

Ruddiman, W. F. and CLIMAP Project Members: Stable isotope data of the 120 k time slice, PANGAEA, doi:10.1594/PANGAEA.51932, 1997. 2539

Rüggeberg, A., Dorschel, B., Dullo, W-C., and Hebbeln, D.: Stable isotope ratios of benthic foraminifera from sediment core GeoB6719-1, PANGAEA, doi:10.1594/PANGAEA.134555, 2005. 2539

Russon, T., Elliot, M., Kissel, C., Cabioch, G., De Deckker, P., and Corrège, T.: Middle-late Pleistocene deep water circulation in the southwest subtropical Pacific, Paleoceanography, 24, doi:10.1029/2009PA001755, 2009. 2539

Sarnthein, M. and Voelker, A.: Stable isotope analysis on sediment core GIK23071-3, PANGAEA, 9, doi:10.1594/PANGAEA.58000, 2001. 2539

Sarnthein, M., Winn, K., Jung, S. J. A., Duplessy, J.-C., Labeyrie, L., Erlenkeuser, H., and Ganssen, G. M.: Changes in east Atlantic deepwater circulation over the last 30 000 years: Eight time slice reconstructions, Paleoceanography, 9, 209–267, 1994. 2499, 2507, 2539

Schmiedl, G. and Mackensen, A.: Late Quaternary paleoproductivity and deep water circulation in the eastern South Altantic Ocean: Evidence from benthic foraminifera, Palaeogeog., Palaeoclim., Palaeoecol., 130, 43–80, 1997. 2539

Schmiedl, G. and Mackensen, A.: Stable oxygen isotope records of different benthic foraminiferal species of core GeoB3004-1 from the western Arabian Sea, PANGAEA, doi:10.1594/PANGAEA.548185, 2006. 2539

Schulz, H., von Rad, U., and Erlenkeuser, H.: Correlation between Arabian Sea and Greenland climate oscillations of the past 110 000 years, Nature, 393, 54–57, 1998. 2539

Shackleton, N. J.: Carbon-13 in Uvigerina: tropical rainforest history and the equatorial Pacific carbonate dissolution cycles, in: The Fate of Fossil Fuel CO_2 in the Oceans, edited by: Anderson, N. R. and Malahoff, A., 401–423, Plenum Press, 1977. 2499

Shackleton, N. J. and Hall, M. A.: Oxygen and carbon isotope stratigraphy of Deep Sea Drilling Project Hole 552A: Plio-Pleistocene glacial history, Initial Rep. of the Deep Sea Drill. Proj., 81, 599–610, 1984. 2511

Shackleton, N. J., Hall, M. A., Line, J., and Cang, S.: Carbon isotope data in core V19-30 confirm reduced carbon dioxide concentration in the ice age atmosphere, Nature, 306, 319–322, 1983. 2499, 2514

Shackleton, N. J., Le, J., Mix, A., and Hall, M. A.: Carbon isotope records from Pacific surface waters and atmospheric carbon dioxide, Quat. Sci. Rev., 11, 387–400, 1992. 2499, 2539

Shackleton, N. J., Hall, M. A., and Pate, D.: Pliocene stable isotope stratigraphy of Site 846, Proc. Ocean Drill. Program Sci. Results, 138, 337–355, 1995. 2539

Shackleton, N. J., Hall, M. A., and Vincent, E.: Phase relationships between millennial-scale events 64 000–24 000 years ago, Paleoceanography, 15, 565–569, doi:10.1029/2000PA000513, 2000. 2539

Sikes, E. L. and Keigwin, L. D.: Equatorial Atlantic sea surface temperature for the last 30 kyr: A comparison of Uk37, δO^{18} and foraminiferal assemblage temperature estimates, Paleoceanography, 9, 31–45, 1994. 2539

Silverman, B. W.: Aspects of the spline smoothing approach to non-parametric regression curve fitting, J. Royal Stat. Soc. Ser. B, 47, 1–52, 1985. 2504, 2505

Sirocko, F.: Sedimentology on core IOE105KK, PANGAEA, doi:10.1594/PANGAEA.77634, 2002. 2539

Sirocko, F., Sarnthein, M., Erlenkeuser, H., Lange, H., Arnold, M., and Duplessy, J.-C.: Century-Scale events in monsoonal climate over the past 24 000 years, Nature, 364, 322–324, 1993. 2539

Sirocko, F., Garbe-Schönberg, D., and Devey, C. W.: Processes controlling trace element geochemistry of Arabian Sea sediments during the last 25 000 years, Glob. and Planetary Change, 26, 217–303, 2000. 2539

Skinner, L. C. and Shackleton, N. J.: An Atlantic lead over Pacific deep-water change across Termination I: implications for the application of the marine isotope stage stratigraphy, Quat. Sci. Rev., 24, 571–580, 2005. 2502

Slowey, N. C. and Curry, W. B.: Glacial-interglacial differences in circulation and carbon cycling within the upper western Atlantic, Paleoceanography, 10, 715–732, 1995. 2539

Spero, H. J. and Lea, D. W.: Intraspecific stable isotope variability in the planktonic foraminifera *Globigerinoides sacculifer*: results from laboratory experiments, Mar. Micropaleontol., 22, 221–234, 1993. 2508

Spero, H. J. and Lea, D. W.: Experimental determination of stable isotope variability in *Globigerina bulloides*: Implications for paleoceanographuc reconstructions, Mar. Micropaleontol., 28, 231–246, 1996. 2509

Thunell, R. C., Qingmin, M., Calvert, S. E., and Pedersen, T. F.: Glacial-Holocene biogenic sedimentation Patterns in the South China Sea: productivity variations and surface water pCO_2, Paleoceanography, 7, 143–162, 1992. 2539

Tian, J., Wang, P. X., Chen, X. R., and Li, Q. Y.: Astronomically tuned Plio-Pleistocene benthic $\delta^{18}O$ records from South China Sea and Atlantic-Pacific comparison, Earth Planet. Sci. Lett., 203, 1015–1029, 2002. 2539

Toggweiler, J. R., Russell, J. L., and Carson, S. R.: Midlatitude westerlies, atmospheric CO_2, and climate change during the ice ages, Paleoceanography, 21, PA2005, doi:10.1029/2005PA001154, 2006. 2516

Venz, K. A., Hodell, D. A., Stanton, C., and Warnke, D. A.: A 1.0 Myr record of glacial North Atlantic intermediate water variability from ODP site 982 in the northeast Atlantic, Paleoceanography, 14, 42–52, 1999. 2539

Voelker, A.: Stable isotopes on Cibicidoides pachyderma of sediment core MD99-2339, PANGAEA, doi:10.1594/PANGAEA.465028, 2006. 2539

Weaver, P. P. E., Carter, L., and Neil., H. L.: Response of surface water masses and circulation to late Quaternary climate change east of New Zealand, Paleoceanography, 13, 70–83, 1998. 2539

Wefer, G., Berger, W. H., Bickert, T., Donner, B., Fischer, G., Kemle-von Mücke, S., Pätzold, J., Meinecke, G., Mller, P. J., Mulitza, S., Niebler, H.-S., Schmidt, H., Schneider, R., and Segl, M.: Late Quaternary surface circulation of the South Atlantic: The stable isotope record and implications for heat transport and productivity, in: The South Atlantic in the late Quaternary: Present and Past Circulation, edited by: Wefer, G., Berger, W. H., Siedler, G., and Webb, D., 461–502, 1996a. 2539

Wefer, G., Berger, W. H., Siedler, G., and Webb, D. (Eds.): The South Atlantic in the late Quaternary: Present and Past Circulation, Springer-Verlag, Berlin, 1996b.

Weinelt, M. and Sarnthein, M.: Stable isotope analysis on sediment core GIK11944-2, PANGAEA, 29, doi:10.1594/PANGAEA.97104, 2003. 2539

Zabel, M., Bickert, T., Dittert, L., and Haese, R. R.: Significance of the sedimentary Al:Ti ratio as an indicator for variations in the circulation patterns of the equatorial North Atlantic, Paleoceanography, 14, 789–799, 1999. 2539

Zahn, R., Winn, K., and Sarnthein, M.: Benthic foraminiferal $\delta^{13}C$ and accumulation rates of organic carbon: *Uvigerina peregrina* group and *Cibicidoides wuellerstorfi*, Paleoceanography, 1, 27–42, 1986. 2539

Zahn-Knoll, R. and Sarnthein, M.: Stable isotope analysis on sediment core GIK15669-1, PANGAEA, doi:10.1594/PANGAEA.106214, 2003a. 2539

Zahn-Knoll, R. and Sarnthein, M.: Stable isotope analysis on sediment core GIK15637-1, PAN-

GAEA, doi:10.1594/PANGAEA.106213, 2003b. 2539
Zhao, M., Beveridge, N. A. S., Shackleton, N. J., Sarnthein, M., and Eglinton, G.: Molecular stratigraphy of cores off northwest Africa: Sea surface temperature history over the last 80 ka, Paleoceanography, 10, 661–675, 1995. 2539

CPD
5, 2497–2554, 2009

Table 1. Cores used in the data synthesis.

Core	Latitude	Longitude	Depth (m)	Ocean	Benthic species	Age (ka)	# of obs.	Sed. rate	Flag	Plank. species	Age (ka)	# of obs.	Sed. rate	Flag	Reference
PS2177-1	88.03	134.93	1388	Arct.						*N. pachyde*	2–76	38	0.6	h	Noer98
PS2185-3	87.52	144.38	1051	Arct.						*N. pachyde*	0–52	34	0.7		Noer98
PS2166-2	86.85	59.77	3636	Arct.						*N. pachyde*	2–73	39	0.6		Noer98
PS2138-1	81.54	30.88	862	Arct.	*C. teretis*	13–150	54	4.2	h						DELPHI
V27-64	73.52	20.00	479	Arct.						*N. pachyde*	10–14	8	75.0		DELPHI
V30-163	72.40	14.82	748	Arct.						*N. pachyde*	24–48	21	46.3		DELPHI
V28-14	64.78	−29.57	1855	Arct.						*N. pachyde*	0–>150	73	3.8		CDLS88
V29-202	61.00	−21.02	2658	Arct.	*C. wueller*	2–>150	184	5.2	p						OL95
V27-60	72.18	−8.58	2525	Arct.^{N}						*N. pachyde*	1–>150	73	4.2		DLB88
					C. wueller	1–133	41	4.2	rH						
PS1243-1	69.37	−6.55	2711	Arct.^{N}	*C. wueller*	1–30	57	2.8		*N. pachyde*	1–30	61	2.8		BESS01
V28-56	68.03	−6.12	2941	Arct.^{N}	*C. wueller*	108–125	9	2.9	P	*N. pachyde*	108–135	13	2.6		CLIMAP
					O. tener	108–125	9	2.9	P						
GIK23071	67.08	2.91	1308	Arct.^{N}							2–140	269	5.3		SV01
SO82_5-2	59.19	−30.90	1416	N Atl.	*C. wueller*	5–65	142	9.7	p	*N. pachyde*	5–47	72	9.4		Jung04
BOFS17K	58.00	−16.50	1150	N Atl.	*C. wueller*	2–49	35	2.8		*G. bulloid*	2–115	121	2.1		LMC94
ODP982	57.50	−15.88	1145	N Atl.	Cib. spp.	0–>150	62	2.5		*G. bulloid*	0–>150	66	2.5		VHSW99
NA87-22	55.50	−14.58	2161	N Atl.	*C. wueller*	0–25	49	25.5							DLAP92
ODP980	55.48	−14.72	2168	N Atl.	*C. wueller*	1–>150	138	14.0							OMC03
GIK17049-6	55.26	−26.73	3331	N Atl.	*C. wueller*	1–>150	123	4.1	h	*G. bulloid*	0–>150	166	4.1	h	JS03
GIK23419-8	54.96	−19.75	1491	N Atl.	*C. wueller*	3–110	147	7.0	h	*G. bulloid*	3–110	158	7.0		JS03b
										N. pachyde	0–41	95	4.0		
V27-20	54.00	−46.20	3510	N Atl.	*C. wueller*	91–148	22	2.3							CLIMAP
GIK23414-9	53.54	−20.29	2196	N Atl.	*C. wueller*	0–>150	178	3.2		Genus mix:	0–>150	182	3.2		JS03c
GIK23415-9	53.18	−19.14	2472	N Atl.	*C. wueller*	1–>150	183	4.0		*G. bulloid*	1–>150	144	4.0		JS03d
NEAP18K	52.77	−30.34	3275	N Atl.	*C. wueller*	55–126	184	5.6	p						CS99
SU90-39	52.57	−21.94	3955	N Atl.	*C. wueller*	10–140	152	6.9	p	*G. bulloid*	10–>150	146	8.0		Cort03
											14–>150	117	8.0	h	
GIK23418-8	52.55	−20.33	1491	N Atl.	*C. wueller*	0–>150	129	6.7	h	*G. bulloid*	0–>150	216	6.7		JS03e
GIK17045-3	52.42	−16.66	3663	N Atl.	*C. wueller*	8–>150	66	4.8	h						SWJD94
GEOB6728-1_ISO	52.15	−12.77	749	N Atl.	*C. kullenb*	2–48	80	9.6							DHRD05
GEOB6719-1	52.15	−12.77	758	N Atl.	*C. kullenb*	13–130	79	3.5							RDDH05
GIK23416-4	51.57	−20.00	3616	N Atl.	*C. wueller*	6–150	90	7.1	h	*G. bulloid*	6–150	144	7.1		JS04a
GIK23417-1	50.67	−19.43	3850	N Atl.	*C. wueller*	4–79	142	7.5		*N. pachyde*	6–79	111	7.6		JS03f
ODP851	46.22	−34.32	3760	N Atl.						*G. sacculi*	4–>150	25	1.9	rh	CR97
NO79-28	45.63	−22.75	3625	N Atl.	*U. peregri*	18–>150	105	5.0	H	*G. bulloid*	10–>150	67	5.0		Dupl96
V29-179	44.71	−24.53	3331	N Atl.	Uvig. spp.	20–150	74	4.1	h						CLIMAP
					C. wueller	2–130	34	4.0	rH						
					M. barlean	14–100	11	4.3	RH						
					H. elegans	2–16	8	3.6							
					Cib. spp.	2–9	4	2.2							
SU90-11	44.07	−40.02	3645	N Atl.	*C. wueller*	10–>150	67	3.6	h	*N. pachyde*	10–150	139	3.6		LVCP95
					U. excelle	12–149	108	3.6	h	*G. bulloid*	10–150	109	3.6		
CHN82-20	43.50	−29.87	3020	N Atl.	*P. wueller*	4–25	49	6.1		*G. bulloid*	4–23	43	6.1		DELPHI
MD952039	40.58	−10.35	3381	N Atl.	*C. wueller*	5–>150	173	10.8							LCO06
NO82-13	40.53	−10.43	3780	N Atl.	*C. wueller*	10–34	43	17.4		*G. bulloid*	10–65	77	14.5		Labe96
PO200_10_6-2	37.82	−9.50	1086	N Atl.	Uvig. spp.	2–41	46	14.4		*G. bulloid*	2–41	47	14.4		ABHR98
MD95-2042	37.80	−10.17	3146	N Atl.	*C. wueller*	2–150	258	20.1							SHV00
PO200/10_8-2.97	37.64	−9.93	2200	N Atl.	*C. wueller*	3–30	23	10.5		*G. bulloid*	2–30	31	10.7		ABHR98
KF09	37.11	−32.29	2655	N Atl.	*C. wueller*	2–31	12	16.0	h	*G. ruber*	2–31	45	16.0		Rich01

Table 1. Continued.

Core	Latitude	Longitude	Depth (m)	Ocean	Benthic species	Age (ka)	# of obs.	Sed. rate	Flag	Plank. species	Age (ka)	# of obs.	Sed. rate	Flag	Reference
MD99-2339	35.89	−7.53	1177	N Atl.	benthic	2–47	184	40.4	p	*N. pachyde*	2–47	182	40.4		Voel06
					Uvig spp.	2–47	52	40.3	P						
V10-58	35.67	26.30	2283	N Atl.						*G. ruber*	1–36	42	15.1		CLIMAP
GIK11944-2	35.65	−8.06	1765	N Atl.	*C. wueller*	10–95	67	6.4							WS03
GIK15669-1	34.89	−7.82	2022	N Atl.	*C. wueller*	9–95	71	5.6							ZS03
GIK15672-1	34.86	−8.13	2460	N Atl.	*C. wueller*	4–57	42	4.3		*G. ruber*	4–55	40	4.3		SWJD94
EN120_GGC_1	33.67	−57.62	4450	N Atl.	Cib spp.	6–25	43	13.9							Keig04
KNR140-51GGC	32.78	−76.12	1790	N Atl.	*U. peregri*	5–18	41	32.3		*G. sacculi*	5–18	44	32.3		Keig04
KNR140-64GGC	32.74	−76.13	2101	N Atl.	*C. wueller*	14–24	18	13.8		*G. ruber*	2–29	52	13.9		Keig04
					U. peregri	1–23	12	13.9	h						
KNR140-67JPC	32.74	−76.13	2102	N Atl.	*N. umbonif*	10–30	32	10.8	p	*G. ruber*	10–29	22	11.2		Keig04
KNR140-43GGC	32.02	−76.07	2590	N Atl.	*U. peregr*	12–22	39	17.7		*G. ruber*	10–25	66	17.7		Keig04
KNR140-37JPC	31.41	−75.26	3000	N Atl.	Cib. spp.	0–149	236	13.5							Keig04
					Uvig. spp.	8–61	164	22.8							
KNR140-30GGC	30.73	−74.47	3433	N Atl.	*U. peregri*	11–24	27	15.8		*G. ruber*	10–25	38	16.0		Keig04
GEOB4216-1	30.63	−12.40	2324	N Atl.	*C. wueller*	4–>150	127	4.5		*G. bulloid*	4–>150	130	4.5		FMHK02
GIK16004-1	29.98	−10.65	1512	N Atl.	*C. wueller*	4–139	60	3.3		*G. bulloid*	4–139	59	3.3		SWJD94
					Pyrgo murr	4–136	32	3.2	r	*G. ruber*	4–139	57	3.3		
										G. inflata	4–128	53	3.3		
GIK15627-3	29.17	−12.09	1024	N Atl.	*C. wueller*	9–>150	49	3.2		*G. inflata*	7–>150	39	3.2	rh	SWJD94
KNR140-12JPC	29.07	−72.90	4250	N Atl.	*N. umbonif*	8–25	43	12.8		*G. ruber*	8–24	32	13.0		Keig04
GEOB4223-2	29.02	−12.47	775	N Atl.	*U. peregri*	1–98	150	7.8		*G. bulloid*	1–98	149	7.8		FMHK02
GEOB4240-2	28.89	−13.22	1358	N Atl.	*C. wueller*	5–137	59	4.9		*G. bulloid*	3–137	133	5.0		FMHK02
KNR140-22JPC	28.02	−74.41	4712	N Atl.	*N. Umbonif*	12–21	20	17.3	P	*G. ruber*	9–21	43	17.3		Keig04
GIK15637-1	27.00	−18.99	3849	N Atl.	*C. wueller*	10–>150	41	2.0	rh						ZS03b
OCE205-149GGC	26.26	−77.67	423	N Atl.	*C. kullenb*	8–44	26	6.8							SC95
OCE205-7JPC	26.14	−77.23	1320	N Atl.	*C. kullenb*	0–69	26	2.6							SC95
					H. elegans	0–137	35	2.0	r						
OCE205-103GCC	26.07	−78.07	965	N Atl.	*C. cicatri*	3–62	42	4.6	p						SC95
					C. kullenb	3–61	100	4.6	p						
OCE205-108GGC	25.98	−78.18	743	N Atl.	*P. arimine*	6–22	28	15.2							SC95
					C. pachyde	0–23	33	10.7							
OCE106GGC	25.98	−78.18	423	N Atl.	*C. cicatri*	6–25	23	7.5							SC95
					C. corpule	6–25	21	7.5							
					C. pachyde	6–25	20	7.5							
					H. elegans	6–25	23	7.5							
					P. arimine	6–25	23	7.5							
					P. foveola	6–22	10	7.5							
					P. roberts	6–25	22	7.5							
GIK12392-1	25.17	−16.84	2575	N Atl.	*C. wueller*	3–141	113	6.9							ZWS86
BOFS28K	24.64	−22.81	4900	N Atl.	*C. wueller*	4–30	20	1.9	P						BES95
BOFS26K	24.48	−19.89	3680	N Atl.	*C. wueller*	4–26	20	1.9							BES95
GIK16017-2	21.25	−17.80	812	N Atl.	*C. wueller*	6–37	57	13.2		*G. ruber*	6–38	55	13.1		SWJD94
GIK16030-1	21.23	−18.05	1516	N Atl.	*C. wueller*	4–109	65	9.6		*G. bulloid*	4–38	43	8.6		SWJD94
					U. peregri	4–35	28	8.4		*G. ruber*	4–38	43	8.6		
										G. inflata	4–38	43	8.6		
GIK12328-5	21.14	−18.57	2798	N Atl.	*C. wueller*	0–47	67	11.8		*G. ruber*	0–49	65	11.9		SWJD94
ODP658C	20.75	−18.58	2273	N Atl.	*C. wueller*	0–50	120	12.6		*G. bulloid*	0–50	113	12.6		ZBSS95
										G. inflata	0–50	118	12.6		
										G. ruber	0–50	120	12.6		
										G. ruber	0–49	113	12.6		
BOFS29K	20.53	−21.11	4000	N Atl.	*C. wueller*	0–32	26	2.8							BES95

Table 1. Continued.

Core	Latitude	Longitude	Depth (m)	Ocean	Benthic species	Age (ka)	# of obs.	Sed. rate	Flag	Plank. species	Age (ka)	# of obs.	Sed. rate	Flag	Reference
V30-49	18.43	−21.10	3093	N Atl.						*C. wueller*	2–28	30	4.3		CDLS88
GIK13289-2	18.07	−18.01	2485	N Atl.	*C. wueller*	3–31	30	6.5							SWJD94
					U. peregri	3–31	26	6.5							
GIK12337-4AND 5	15.95	−18.13	3094	N Atl.	*C. wueller*	10–17	28	19.5		*G. ruber*	10–17	28	19.5		SWJD94
GIK16402-1	14.42	−20.57	4203	N Atl.	*C. wueller*	6–>150	33	2.1	rh	*G. sacculi*	5–22	12	3.9		SWJD94
V22-197	14.17	−18.58	3167	N Atl.	Uvig. spp.	1–>150	87	5.1							CDLS88
GIK13239-1	13.88	−18.31	3156	N Atl.	*C. wueller*	8–40	48	13.7							SWJD94
					U. hollick	8–40	45	13.7							
V22-196	13.83	−18.96	3728	N Atl.	*C. wueller*	3–19	13	5.1							CLIMAP
M35003-4	12.09	−61.24	1299	N Atl.	Cib. spp.	1–57	96	16.6	P						Huel99
					Uvig. spp.	24–58	53	16.6	P						
V22-108	9.92	−20.98	4956	N Atl.						*G. bulloid*	1–133	29	4.1	rH	CLIMAP
GIK16408-2	9.01	−21.46	4239	N Atl.	*C. wueller*	2–18	10	2.3		*G. ruber*	0–18	12	2.3		SWJD94
GIK16408-5	9.01	−21.50	4336	N Atl.	*C. wueller*	2–27	11	2.2							SWJD94
GIK16459-1	7.28	−26.19	4835	N Atl.	*C. wueller*	8–36	30	3.1		*G. ruber*	8–21	18	3.1		SWJD94
GEOB4403-2	6.13	−43.44	4503	N Atl.	*C. wueller*	1–>150	136	3.4	H						BM03
ODP929	5.98	−43.74	4356	N Atl.	*C. wueller*	10–>150	52	5.8							BCW97
					C. cicatri	24–>150	11	5.6	RH						
GIK13519-1	5.67	−19.85	2862	N Atl.	*C. wueller*	1–>150	79	1.3							SWJD94
					U. hollick	13–144	34	1.4	rh						
ODP927	5.46	−44.48	3315	N Atl.	*C. wueller*	10–>150	56	5.3	P						CO05
					Cib. spp.	26–>150	11	5.3	RHP						
EW9209-1JPC	5.00	−43.00	4056	N Atl.	*C. wueller*	1–150	229	3.8	p						CO97
KN11002-0055	4.95	−42.89	4556	N Atl.	*C. wueller*	5–63	40	2.2							CDLS88
KN11002-0050PG	4.87	−43.20	3995	N Atl.	*C. wueller*	12–47	40	3.8	p						CDLS88
GIK16856-2	4.80	3.40	2861	N Atl.		8–74	43	4.7							SWJD94
KN11002-0058	4.79	−43.04	4341	N Atl.	*C. wueller*	4–43	38	3.3							CDLS88
KN11002-0066PG	4.56	−43.38	3547	N Atl.	*C. wueller*	2–39	40	3.6							CDLS88
GEOB1520-1	4.49	−41.93	3911	N Atl.	*C. wueller*	6–>150	80	1.8							BM03
KN11002-0071PG	4.36	−43.70	3164	N Atl.	*C. wueller*	1–42	44	3.5							CDLS88
KN11002-0075	4.34	−43.41	3063	N Atl.	*C. wueller*	4–72	40	1.9							CDLS88
ODP925	4.20	−43.49	3041	N Atl.	*C. wueller*	10–>150	39	4.3	rH						BCW97
					C. bradyii	18–>150	18	4.2	RH						
GEOB1523-2	3.83	−41.62	3291	N Atl.	*C. wueller*	2–>150	61	2.0							Muli98
GIK13521-1	3.02	−22.03	4504	N Atl.	*C. wueller*	7–>150	25	2.4	rH	*G. sacculi*	7–>150	27	2.7	rh	SWJD94
GEOB1505-2	2.27	−33.02	3706	N Atl.											ZBDH99
					C. wueller	10–>150	63	2.0							
GEOB1101-5	1.66	−10.98	4588	N Atl.	*C. wueller*	8–>150	36	1.4	r						BW96
GIK16771-2	0.82	−15.51	2764	N Atl.	*C. wueller*	4–87	11	2.1	RH	*G. sacculi*	4–>150	30	2.0	rh	SWJD94
										G. ruber	4–>150	30	2.0	rh	
12PC51	0.01	−23.00	3870	N Atl.						*G. sacculi*	9–47	44	2.5		SK94
GEOB2215-10	0.01	−23.50	3711	N Atl.	*C. wueller*	8–30	24	5.5							BM03
GIK16773-1	−0.97	−9.44	4662	S Atl.	*C. wueller*	0–17	29	3.3		*G. ruber*	0–17	29	3.3		SWJD94
GIK16772-1	−1.34	−11.97	3911	S Atl.	*C. wueller*	14–>150	56	4.6		*G. sacculi*	14–>150	58	4.6		SWJD94
GIK12329-6	−1.35	−19.93	3912	S Atl.	*C. wueller*	4–43	23	3.1							SWJD94
					Pyrgo spp.	70–>150	25	2.8	r						
GEOB1105-4	−1.67	−12.43	3225	S Atl.	*C. wueller*	8–>150	123	4.1							BW96
GIK16867-2	−2.20	5.10	3891	S Atl.	*C. wueller*	8–137	48	2.7		*G. ruber*	8–137	50	2.7		SWJD94
RC13-205	−2.29	5.18	3731	S Atl.						*G. ruber*	3–22	11	6.3		CLIMAP
GEOB1041-3	−3.48	−7.60	4033	S Atl.							5–>150	56	2.1		BW96
GEOB1118-2	−3.56	−16.43	4675	S Atl.	*C. wueller*	6–>150	67	2.1	P						BW96
GEOB1115-3	−3.56	−12.56	2945	S Atl.	*C. wueller*	1–>150	102	3.2	P						BW96
GEOB1501-4	−3.68	−32.01	4257	S Atl.	*C. wueller*	10–28	14	3.6							DHMP97
GEOB1112-4	−5.78	−10.75	3125	S Atl.	*C. wueller*	3–>150	74	2.6	P						BW96

Table 1. Continued.

Core	Latitude	Longitude	Depth (m)	Ocean	Benthic species	Age (ka)	# of obs.	Sed. rate	Flag	Plank. species	Age (ka)	# of obs.	Sed. rate	Flag	Reference
V12-70	−6.48	11.43	450	S Atl.	*P. arimine*	12–43	28	6.4		*G. sacculi*	12–43	28	6.4		LCO06
GEOB1903-3	−8.68	−11.85	3161	S Atl.	*C. wueller*	8–30	15	3.2	P						DHMP97
V22-38	−9.55	−34.25	3797	S Atl.	*C. wueller*	78–135	16	1.4	rhp	*G. sacculi*	78–135	35	1.4		CLIMAP
V22-174	−10.07	−12.82	2630	S Atl.	Uvig. spp.	0–130	41	2.4	r						MRKM89
ODP1079	−11.93	13.31	755	S Atl.	*C. pachyde*	0–20	34	42.5							LCO06
					Planulina	0–20	29	26.4							
GEOB1417-1	−15.54	−12.71	2845	S Atl.	*C. wueller*	10–23	14	5.0							BM03
V29-135	−19.70	8.88	2675	S Atl.	*C. wueller*	4–>150	57	3.4	hp						SWJD94
GEOB1028-5	−20.10	9.19	2209	S Atl.	*C. wueller*	3–>150	90	2.6							WBBD96
V19-258	−20.40	11.62	965	S Atl.	*C. pachyde*	8–29	20	11.3		*G. bulloid*	8–30	40	11.1		LCO06
GEOB5115-2	−21.14	−14.04	3291	S Atl.	*C. wueller*	4–23	22	1.1							BM03
GEOB1035-3	−21.60	5.03	4450	S Atl.	*C. wueller*	6–>150	37	1.3	rP						BW96
GEOB3202-1	−21.62	−39.98	1090	S Atl.	*U. peregri*	10–62	98	9.4		*G. sacculi*	10–62	98	9.4		APW99
										G. ruber	10–62	99	9.4		
GEOB1034-3	−21.73	5.42	3772	S Atl.	*C. wueller*	7–>150	33	0.8	r						BW96
RC13-228	−22.33	11.20	3204	S Atl.	*C. wueller*	1–136	54	5.0	HP						CDLS88
					Uvig. spp.	116–150	10	3.4	rhP						
GEOB1032-3	−22.91	6.04	2505	S Atl.	*C. wueller*	6–>150	43	1.4	rP						BW96
GEOB1710-3	−23.43	11.70	2987	S Atl.	*C. wueller*	2–>150	151	5.4							SM97
RC8-39	−24.07	−15.12	3977	S Atl.						*G. bulloid*	10–136	52	7.0	H	CLIMAP
GEOB1211-3	−24.47	7.54	4089	S Atl.	*C. wueller*	6–>150	37	0.7	rhP						BW96
V19-248	−24.57	4.83	3321	S Atl.						*G. ruber*	5–32	8	1.8	r	CLIMAP
GEOB1214-1	−24.69	7.24	3210	S Atl.	*C. wueller*	3–>150	35	1.2	r						SM97
RC13-229	−25.49	11.31	4191	S Atl.	Uvig. spp.	1–>150	37	2.2	rhP						OFGS90
ODP1084B	−25.51	13.03	1992	S Atl.	*C. wueller*	7–19	18	26.5							LCO06
GEOB2109-1	−27.91	−45.88	2504	S Atl.	*C. wueller*	6–>150	106	2.7							DHMP97
V20-220	−28.60	−29.02	3601	S Atl.	Orid. spp.	15–27	7	20.5							DELPHI
										G. pseudoa	21–27	8	20.5		
GEOB1721-6	−29.17	13.08	3044	S Atl.	*C. wueller*	0–>150	78	2.6							BM03
GEOB1722-3	−29.49	11.75	3973	S Atl.	*C. wueller*	1–>150	50	1.3							MSMS02
GEOB3801-6	−29.51	−8.31	4546	S Atl.	*C. wueller*	8–>150	33	1.3	r						BM03
V19-240	−30.58	13.28	3103	S Atl.	*C. wueller*	2–35	13	3.1							LCO06
GEOB2004-2	−30.87	14.34	2569	S Atl.	*C. wueller*	4–30	33	6.2							BM03
ODP1087	−31.46	15.31	1372	S Atl.	*C. wueller*	0–>150	69	2.5							PSUG01
GEOB1312-2	−31.66	−29.66	3436	S Atl.	*C. wueller*	9–>150	23	0.9	Rp	*G. ruber*	9–>150	23	0.9	R	HP99
V19-236	−33.88	17.63	280	S Atl.	*C. pachyde*	9–26	34	20.0		*G. bulloid*	9–26	34	20.0		LCO06
					P. arimine	8–26	20	20.0							
GEOB3603-2	−35.13	17.54	2840	S Atl.	*C. wueller*	12–>150	87	3.2							BM03
RC11-86	−35.78	18.45	2829	S Atl.						*G. sacculi*	7–27	14	3.2		CLIMAP
					Var. benth	7–27	14	3.2							
GEOB2019-1	−36.06	−8.78	3825	S Atl.	*C. wueller*	6–30	14	2.9	P						BM03
MD96-2080	−36.27	19.48	2488	S Atl.	*C. wueller*	1–>150	35	1.9	rp	*G. inflata*	1–>150	35	1.9	r	RRLG02
RC12-294	−37.27	−10.12	3308	S Atl.	Uvig. spp.	13–>150	73	2.9							IMM97
					C. wueller	16–>150	19	2.8	RH						
RC12-267	−38.68	−25.78	4144	S Atl.						Uvig. spp.	9–20	7	9.2		CLIMAP
ODP1089	−40.94	9.89	4621	S Atl.^{S}	Cib. spp.	3–>150	382	15.5	p	*G. bulloid*	1–>150	400	15.4		HVCN03
ODP1088	−41.14	13.56	2082	S Atl.^{S}	Cib. spp.	3–>150	29	1.3	rhp						HVCN03
PS2495-3	−41.27	−14.49	3134	S Atl.^{S}	Cib. spp.	10–>150	43	3.0	r						MGHK94
ODP1090	−42.91	8.90	3702	S Atl.^{S}	Cib. spp.	6–145	79	3.5	h						HVCN03
					C. wueller	6–>150	79	2.0	h	*G. bulloid*	5–>150	168	2.0		
					C. kullenb	7–>150	60	3.0	H						
										N. pachyde	7–>150	151	3.0		
RC15-94	−42.98	−20.86	3762	S Atl.^{S}						*G. inflata*	9–29	25	12.1		CLIMAP
PS2082-1	−43.22	11.74	4610	S Atl.^{S}	Cib. spp.	10–>150	68	4.4	hp	*N. pachyde*	10–>150	71	4.4		MGHK94

Table 1. Continued.

Core	Latitude	Longitude	Depth (m)	Ocean	Benthic species	Age (ka)	# of obs.	Sed. rate	Flag	Plank. species	Age (ka)	# of obs.	Sed. rate	Flag	Reference
										G. bulloid	10–>150	71	4.4		
PS2498-1	−44.15	−14.23	3783	S Atl.^{S}	Cib. spp.	6–135	96	9.0							MRK01
ODP704A	−46.88	7.42	2543	S Atl.^{S}	Cib. spp.	9–>150	18	2.8	RHp	*N. pachyde*	9–>150	26	2.8	rh	HVCN03
					Gyroidina	9–>150	19	2.8	Rhp						
RC13-269	−52.63	0.12	2591	S Atl.^{S}	Uvig. spp.	9–90	40	6.1	p						CLIMAP
PS1506	−68.73	−5.85	2426	S Atl.^{S}	*E. Exigua*	0–>150	67	0.8	h	*N. pachyde*	0–>150	82	0.8		RERH09
M5-3A-422	24.39	58.04	2732	Ind.	*C. wueller*	1–25	91	9.2		*G. ruber*	0–24	84	9.3		SGD00
SO90-93K	23.59	64.22	1802	Ind.						*G. ruber*	36–68	50	3.3		SVE98
										G. ruber	68–81	44	8.1		
ORGON4-KS8	23.47	59.19	2900	Ind.	*C. wueller*	10–39	61	19.9		*G. ruber*	10–36	58	21.1		SGD00
V34-88	16.54	59.76	2171	Ind.	Uvig. spp.	100–144	24	3.5	p	*G. sacculi*	100–144	32	3.5		CLIMAP
SK17	15.25	72.73	840	Ind.						*G. ruber*	4–25	58	2213.0		Anandpc
										G. bulloid	4–25	57	2213.0		
GEOB3004-1	14.61	52.92	1803	Ind.	*C. wueller*	0–>150	163	5.3							SM06
SO42-74KL	14.33	57.35	3212	Ind.											SSEL93
					C. wueller	1–47	107	6.7	p	*G. ruber*	1–47	123	6.7		
IOE105KK	11.27	53.54	3535	Ind.						*G. ruber*	2–30	20	6.8		Siro02
905	10.46	51.56	1580	Ind.	*C. wueller*	0–26	27	23.3		*G. ruber*	0–26	31	23.3		JKGP09
										G. bulloid	0–26	31	23.3		
RC12-339	9.13	90.03	3010	Ind.	*C. wueller*	99–138	22	1.8		*G. sacculi*	99–138	36	1.8		CLIMAP
V19-178	8.12	73.27	2188	Ind.						*G. ruber*	7–25	8	3.6		PHWB80
V19-188	6.87	60.67	3356	Ind.						*G. ruber*	3–30	16	3.2		CLIMAP
										G. sacculi	2–30	17	3.2		
V29-29	5.12	77.58	2673	Ind.						*G. sacculi*	83–147	37	2.8		CLIMAP
MD900963	5.05	73.90	2446	Ind.							10–>150	86	4.4		BBVL94
V29-31	3.80	78.65	3793	Ind.						*G. menardi*	5–15	11	10.0		DELPHI
RC14-37	1.47	90.17	2226	Ind.						*G. ruber*	10–21	10	6.4		CLIMAP
MD01-2378	−13.08	121.79	1783	Ind.	*C. wueller*	0–150	156	10.5	p						KHK06
RC17-98	−13.22	65.62	3409	Ind.						*G. sacculi*	108–>150	17	2.3		CLIMAP
V28-345	−17.67	117.95	1904	Ind.	Uvig. spp.	102–150	8	2.1	RHp	*G. sacculi*	100–150	26	2.1		CLIMAP
						125–150	10	2.4	p						
						117–146	9	2.2	rp						
182-1132B	−33.32	127.60	219	Ind.	*U. peregri*	18–>150	52	36.3							HKJ02
E49-21	−42.18	94.90	3328	Ind.^{S}						planktonic	2–>150	28	1.9	rh	CLIMAP
RC08-39	−42.88	42.35	4330	Ind.^{S}						*G. bulloid*	114–137	30	6.4		CLIMAP
RC11-120	−43.31	79.52	3193	Ind.^{S}	Uvig. spp.	3–115	63	3.5	p						MPHI87
					Globocas.	3–115	37	3.5	rhp						
					C. wueller	3–130	34	3.4	rHp						
										G. bulloid	3–>150	98	3.2		
ELT45029-PC	−44.88	106.52	3867	Ind.^{S}						*G. bulloid*	10–>150	33	3.1	r	CLIMAP
MD88-770	−46.02	96.46	3290	Ind.^{S}	*C. wueller*	7–17	9	9.1	p						Labe98
ELT49018-PC	−46.05	90.16	3282	Ind.^{S}						*G. bulloid*	12–140	56	4.3		CLIMAP
E49-23	−47.12	95.10	3206	Ind.^{S}						planktonic	4–118	57	5.1		HP94
ELT49023-PC	−47.13	95.08	3285	Ind.^{S}							12–116	57	5.5		HP94
ELT49017-PC	−48.28	90.25	3546	Ind.^{S}						*G. bulloid*	18–>150	46	2.2		HP94
V36-06	19.43	115.90	2387	N Pac.^{SC}						*G. sacculi*	0–109	112	10.9		DELPHI
GGC-6	12.15	118.06	2975	N Pac.^{SC}						*G. sacculi*	8–50	30	3.5		TQCP92
GGC-12	11.93	118.21	2495	N Pac.^{SC}							6–36	28	4.6		TQCP92
GGC-11	11.89	118.33	2165	N Pac.^{SC}						*G. sacculi*	6–40	29	4.1		TQCP92
GGC-10	11.72	118.51	1605	N Pac.^{SC}						*G. sacculi*	4–37	29	4.4		TQCP92
GGC-13	10.60	118.29	990	N Pac.^{SC}						*G. sacculi*	1–33	30	4.5		TQCP92

Table 1. Continued.

Core	Latitude	Longitude	Depth (m)	Ocean	Benthic species	Age (ka)	# of obs.	Sed. rate	Flag	Plank. species	Age (ka)	# of obs.	Sed. rate	Flag	Reference
ODP1143	9.36	113.29	2772	N Pac.[SC]	*C. wueller*	5–147	60	6.7	h						TWCL02
V35-05	7.20	112.08	1953	N Pac.[SC]	*C. wueller*	2–19	12	20.5							OF87
RC23-50B	1.03	104.41	3473	N Pac.[SC]	Uvig. spp.	8–15	21	5.0	p						DELPHI
V32-161	48.28	149.07	1600	N Pac.	Uvig. spp.	0–48	24	5.0	h						MHS91
Y2711-1	43.26	−126.38	2913	N Pac.	Uvig. spp.	112–142	37	5.2							CLIMAP
J-11	40.13	−134.00	1150	N Pac.						*N. pachyde*	6–28	61	6.6		GS00
V32-128	36.47	177.17	3623	N Pac.	*C. wueller*	0–>150	34	2.7	rh						CLIMAP
					Uvig. spp.	2–>150	5	3.6	RH						
V32-126	35.32	177.92	3870	N Pac.	Var. benth	3–133	18	4.6	RH						CLIMAP
RC10-175	34.58	159.17	4014	N Pac.	Var. benth	8–20	6	3.8							DELPHI
V28-304	28.53	134.13	2942	N Pac.	*C. wueller*	0–>150	46	4.5	rh						CDLS88
					Uvig. spp.	0–>150	62	4.5	h						
					Cib. spp.	8–37	15	6.6							
V28-294	28.43	139.97	2308	N Pac.	Uvig. spp.	31–80	26	4.7							CLIMAP
RC12-36	14.74	−97.67	3354	N Pac.	Uvig. spp.	12–19	6	2.7	p						DELPHI
V28-240	5.22	158.07	1767	N Pac.						*G. fistulo*	24–46	49	21.8		DELPHI
V28-179	4.62	−139.60	4502	N Pac.	*Globocas.*	18–107	107	2.4							DELPHI
RC17-176	3.75	158.77	3156	N Pac.						*G. sacculi*	17–26	18	0.4		DELPHI
V17-42	3.53	−81.18	1814	N Pac.						*G. ruber*	12–21	5	5.8		DELPHI
										G. sacculi	9–21	7	5.8		
V19-25	2.47	−81.70	2404	N Pac.						*G. dutertr*	6–37	40	6.3		DELPHI
RC13-138	1.81	−94.14	2655	N Pac.						*G. sacculi*	1–>150	201	4.8		DELPHI
ODP805C	1.23	160.53	3188	N Pac.	*C. wueller*	16–>150	18	1.3	Rhp						LPS00
V28-238	1.02	160.48	3120	N Pac.						*G. sacculi*	3–>150	48	1.8	r	CLIMAP
V21-29	0.95	−89.35	712	N Pac.	Uvig. spp.	3–23	9	8.0	p						DELPHI
V24-109	0.43	158.80	2367	N Pac.	*C. wueller*	0–80	103	3.4	p						SLMH92
										G. sacculi	1–>150	93	1.4		
ODP806B	0.32	159.36	2520	N Pac.	*C. wueller*	3–>150	31	2.6	rhp	*G. sacculi*	3–>150	31	2.9	rh	LPS00
RC13-110	0.00	−96.02	3231	N Pac.	*C. wueller*	5–>150	63	2.0	h						MPZR91
V19-27	−0.47	−82.08	1373	S Pac.											MPZR91
					C. wueller	3–150	71	2.5							
RC10-65	−0.69	−108.62	3588	S Pac.						*G. sacculi*	11–20	21	6.7		DELPHI
										Pulleniati	11–20	24	7.8		
										G. tumida	11–45	47	11.7		
RC10-97	−0.92	−134.31	4305	S Pac.	Var. benth	5–25	6	2.4	r						DELPHI
V19-28	−2.37	−84.65	2720	S Pac.	Uvig. spp.	0–>150	67	4.4	p						DELPHI
RC10-140	−2.65	156.98	1679	S Pac.						*G. sacculi*	14–30	10	5.6		DELPHI
ODP846	−3.08	−90.83	3296	S Pac.	*C. wueller*	8–>150	56	3.7							SHP95
					U. peregri	99–>150	14	3.7	r						
V19-30	−3.57	−83.23	3157	S Pac.	benthic	0–>150	297	5.3	p						CDLS88
V28-235	−5.45	160.48	1746	S Pac.						*G. sacculi*	2–>150	26	1.3	r	CLIMAP
V24-184	−12.87	146.22	2992	S Pac.						*G. sacculi*	5–>150	15	1.3	Rh	APB89
V24-170	−13.52	146.90	2243	S Pac.						*G. sacculi*	2–>150	21	1.4	R	APB89
RC10-131	−14.53	157.97	2933	S Pac.						*G. sacculi*	3–65	25	3.9		APB89
MW91-15	−14.53	157.98	3296	S Pac.						*G. sacculi*	4–34	32	2.1		PT97
V24-166	−16.52	150.78	781	S Pac.						*G. sacculi*	2–10	13	30.0		APB89
V24-161	−18.20	151.47	1670	S Pac.						*G. sacculi*	25–89	19	2.8	r	APB89
MD06-3018	−23.00	166.15	2470	S Pac.	*C. wueller*	4–>150	35	1.6	r						REKC09
RC12-113	−24.88	163.53	2454	S Pac.						*G. sacculi*	8–76	24	3.5		APB89
RC12-109	−25.88	157.88	2930	S Pac.						*G. sacculi*	5–>150	22	1.5	R	APB89
RC15-52	−29.24	−85.98	3780	S Pac.	Uvig. spp.	10–30	11	2.2	p						CLIMAP
CHAT10K-1	−40.03	180.00	3003	S Pac.[S]	Uvig. spp.	0–31	83	10.6	p	*G. bulloid*	0–31	83	10.6		MCH08
										G. inflata	0–31	83	10.6		

CPD

5, 2497–2554, 2009

Title Page
Abstract
Introduction
Conclusions
References
Tables
Figures
Back
Close
Full Screen / Esc
Printer-friendly Version
Interactive Discussion

Table 1. Continued.

Core	Latitude	Longitude	Depth (m)	Ocean	Benthic species	Age (ka)	# of obs.	Sed. rate	Flag	Plank. species	Age (ka)	# of obs.	Sed. rate	Flag	Reference
MD97-2121	−40.38	177.99	3014	S Pac.^{S}	Uvig. spp.	0–140	134	24.8	p	*G. inflata*	0–140	156	24.8		CMGN08
					Cib. spp.	1–132	57	24.9	Hp						
P69	−40.38	178.00	2195	S Pac.^{S}	benthic	6–26	33	30.2	p						WCN98
S794	−40.40	178.00	2195	S Pac.^{S}						*G. bulloid*	0–126	48	0.0		WCN98
CHAT5K	−40.78	−171.55	4240	S Pac.^{S}	Uvig. spp.	6–>150	32	1.0	rhp	*G. bulloid*	11–>150	21	1.0	RH	MCH08
CHAT1K	−41.58	−171.52	3556	S Pac.^{S}	Uvig. spp.	2–>150	84	2.1							WCN98
R657	−42.38	−178.49	3284	S Pac.^{S}	Uvig. spp.	6–>150	26	1.9	r	*G. bulloid*	3–>150	28	1.9	r	WCN98
CHAT3K	−42.66	−167.50	4802	S Pac.^{S}	Uvig. spp.	8–>150	125	1.9	h	*G. bulloid*	8–>150	129	1.9		MCH08
										G. inflata	8–>150	129	1.9		
U938	−45.08	179.50	2700	S Pac.^{S}	Uvig. spp.	5–95	39	0.0	hp	*G. bulloid*	6–95	42	0.0		WCN98
RC15-62	−45.29	−77.21	2809	S Pac.^{S}	Uvig. spp.	10–15	5	7.2	p						DELPHI
MD97-2120	−45.53	174.93	1210	S Pac.^{S}	Genus mix:	2–>150	480	10.7							PZES03
DSDP594	−45.59	175.08	1204	S Pac.^{S}	Uvig. spp.	4–>150	158	12.9	p	*G. bulloid*	4–>150	179	12.9		WCN98
Q200	−45.99	172.03	1370	S Pac.^{S}	benthic	5–120	22	2.4	rhp	planktonic	5–120	32	2.4	r	WCN98
RC12-225	−53.66	−123.13	2964	S Pac.^{S}						*G. bulloid*	8–51	42	8.1		RE99

Abbreviations are as follows. In header rows: Plank=planktonic; # of obs.=number of observations in core; Sed. rate=mean sedimentation rate (cm/kyr) over period of data; all latitudes and longitudes in decimal degrees. In Ocean column: Arct.=Arctic Ocean; Arct^N=Nordic seas; ^{C}=Caribbean Sea; ^{S}=Southern Ocean (defined as >40° S); ^{SC}=South China Sea. In Flag columns; R=mean data resolution poorer than 6 kyr; r=mean data resolution poorer than 3 kyr; H=at least one period of >20 kyr with no obseravtions; h=at least one period of >10 kyr with no observations; P=phytodetritus correction and error applied; p=phytodetritus error only applied. Relevant references are as follows: ABHR98=Abrantes et al. (1998); APB89=Anderson et al. (1989); APW99=Arz et al. (1999); Anandpc=P. Anand (pers. comm.); BBVL94=Bassinot et al. (1994); BCW97=Bickert et al. (1997); BES95=Beveridge et al. (1995); BESS01=Bauch et al. (2001); BM03=Bickert and Mackensen (2003); BW96=Bickert and Wefer (1996); CDLS88=Curry et al. (1988); CLIMAP=Ruddiman and CLIMAP Project Members (1997); CMGN08=Carter et al. (2008); CO05=Curry and Oppo (2005); CO97=Curry and Oppo (1997); CR97=Cannariato and Ravelo (1997); CS99=Chapman and Shackleton (1999); Cort03=Cortijo (2003); DELPHI=Delphi project, http://rock.esc.cam.ac.uk/delphi; DHMP97=Dürkop et al. (1997); DHRD05=Dorschel et al. (2005); DLAP92=Duplessy et al. (1992); DLB88=Duplessy et al. (1988a); Dupl96=Duplessy (1996); FMHK02=Freudenthal et al. (2002); GS00=Gorbarenko and Southon (2000); HKJ02=Holbourn et al. (2002); HP94=Howard and Prell (1994); HP99=Hale and Pflaumann (1999); HVCN03=Hodell et al. (2003); Huel99=Hüls (1999); IMM97=Imbrie et al. (1997); JKGP09=Jung et al. (2009); JS03=Jung and Sarnthein (2004a); JS03b=Jung and Sarnthein (2003a); JS03c=Jung and Sarnthein (2003b); JS03d=Jung and Sarnthein (2003c); JS03e=Jung and Sarnthein (2003d); JS03f=Jung and Sarnthein (2003e); JS04a=Jung and Sarnthein (2004b); Jung04=Jung (2004); KHK06=Kawamura et al. (2006); Keig04=Keigwin (2004); LCO06=Lynch-Stieglitz et al. (2006); LMC94=Lowry et al. (1994); LPS00=Lea et al. (2000); LVCP95=Labeyrie et al. (1995); Labe96=Labeyrie (1996); Labe98=Labeyrie (1998); MCH08=McCave et al. (2008), cores excluded from Supplementary Materials; MGHK94=Mackensen et al. (1994); MHS91=Morley et al. (1991); MPHI87=Martinson et al. (1987); MPZR91=Mix et al. (1991); MRK01=Mackensen et al. (2001); MRKM89=McIntyre et al. (1989); WS03=Weinelt and Sarnthein (2003); MSMS02=Mollenhauer et al. (2002); Muli98=Mulitza (1998); Noer98=Nørgaard-Pedersen et al. (1998); OF87=Oppo and Fairbanks (1987); OFGS90=Oppo et al. (1990); OL95=Oppo and Lehmann (1995); OMC03=Oppo et al. (2003); PHWB80=Prell et al. (1980); PSUG01=Pierre et al. (2001); PT97=Patrick and Thunell (1997); PZES03=Pahnke et al. (2003); RDDH05=Rüggeberg et al. (2005); RE99=Rickaby and Elderfield (1999); REKC09=Russon et al. (2009); RERH09=Rickaby et al. (2009); RRLG02=Rau et al. (2002); Rich01=Richter (2001); SC95=Slowey and Curry (1995); SGD00=Sirocko et al. (2000); SHP95=Shackleton et al. (1995); SHV00=Shackleton et al. (2000); SK94=Sikes and Keigwin (1994); SLMH92=Shackleton et al. (1992); SM06=Schmiedl and Mackensen (2006); SM97=Schmiedl and Mackensen (1997); SSEL93=Sirocko et al. (1993); SV01=Sarnthein and Voelker (2001); SVE98=Schulz et al. (1998); SWJD94=Sarnthein et al. (1994); Siro02=Sirocko (2002); TQCP92=Thunell et al. (1992); TWCL02=Tian et al. (2002); VHSW99=Venz et al. (1999); Voel06=Voelker (2006); WBBD96=Wefer et al. (1996a); WCN98=Weaver et al. (1998); ZBDH99=Zabel et al. (1999); ZBSS95=Zhao et al. (1995); ZS03=Zahn-Knoll and Sarnthein (2003a); ZS03b=Zahn-Knoll and Sarnthein (2003b); ZWS86=Zahn et al. (1986)

Table 2. Species-specific error estimates and uniform adjustments applied to the dataset, excluding those due to changes in the phytodetritus effect in upwelling regions. Correction and correction error estimates affect the calculation of δ^{13}C but not $\Delta_{LGM}\delta^{13}$C; where no correction is given, no δ^{13}C estimate is made.

Species	$\Delta_{LGM}\delta^{13}$C error ($2\sigma_{sp}$),‰	Correction (δ_{csp}),‰	Correction error ($2\sigma_{csp}$),‰
C. wuellerstorfi	0.15	0	0.20
Benthics			
Other *Cibicidoides*	0.35	0	0.28
Uvigerina spp.	0.23	+0.85	0.48
H. elegans or unspecified	0.6	–	–
Other benthic spp.	0.4	–	–
Planktonics			
G. ruber	0.4	0	0.2
G. bulloides	0.4	+2.11	0.32
G. sacculifer	0.4	−0.27	0.2
N. pachyderma	0.4	+0.68	0.39
Other planktonic spp.	0.6	–	–

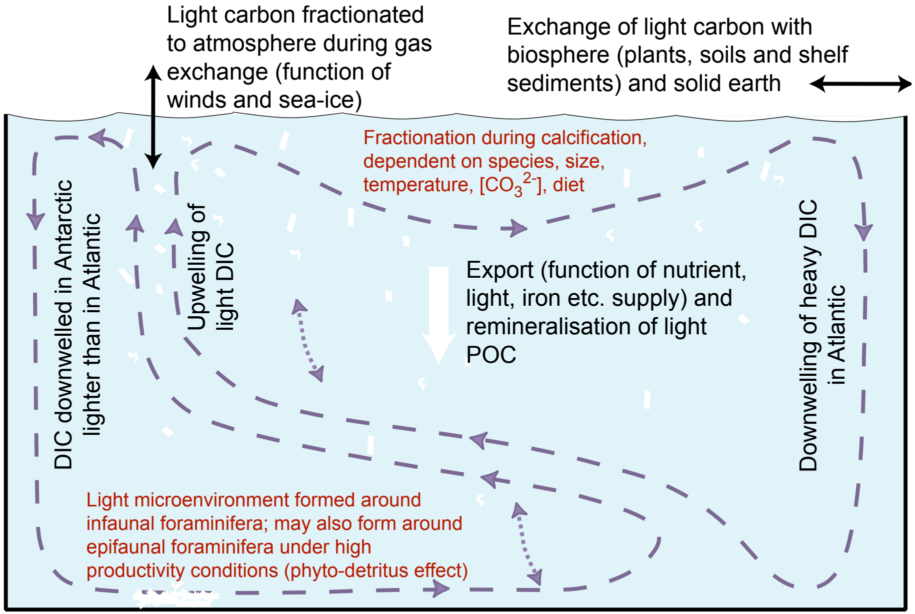

Fig. 1. Schematic of processes influencing $\delta^{13}C$ recorded in calcium carbonate from foraminiferal shells. Processes in large font affect open seawater $\delta^{13}C$; processes in small font affect the difference between recorded $\delta^{13}C$ and water $\delta^{13}C$. DIC≡dissolved inorganic carbon; POC≡particulate organic carbon.

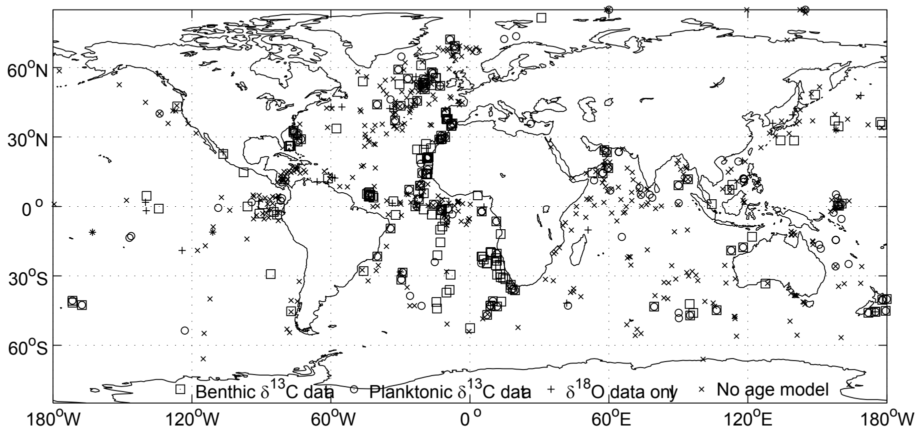

Fig. 2. Core locations of records included in the pre-processed data synthesis, or excluded because no δ^{18}O-derived age model could be constructed. For most excluded records, there were too few data (often true of cores sampled only at the LGM and/or Holocene), or the sampling resolution was targeted at longer timescales than a glacial cycle. The inclusion of records in the pre-processed synthesis was not explicitly constrained by data quality.

CPD
5, 2497–2554, 2009

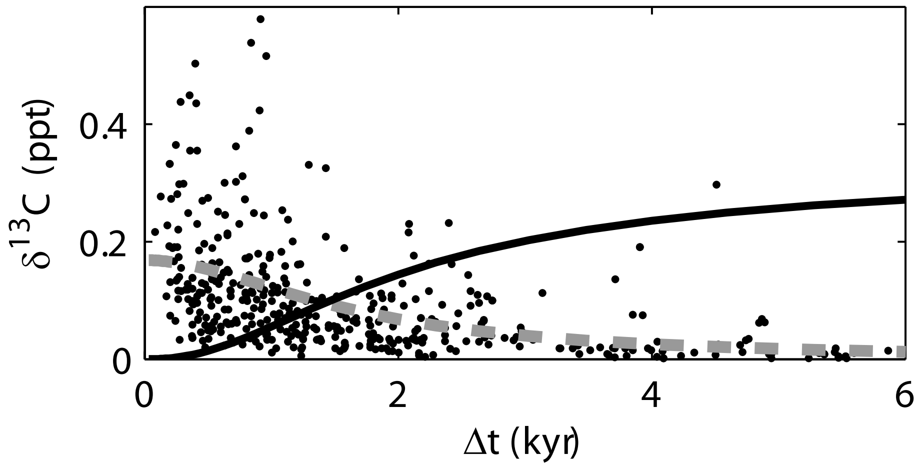

Fig. 3. Estimate of aliasing error, $2\sigma_{\rm ali}$, as a function of data resolution Δt (solid line). Dots are the root-mean-square of the residuals for each record, $\bar{y}'$, as a function of mean data resolution, with a line of best fit, $y'_{\rm h}$ (dashed line). $2\sigma_{\rm ali}$ is calculated using Eq. (5).

CPD
5, 2497–2554, 2009

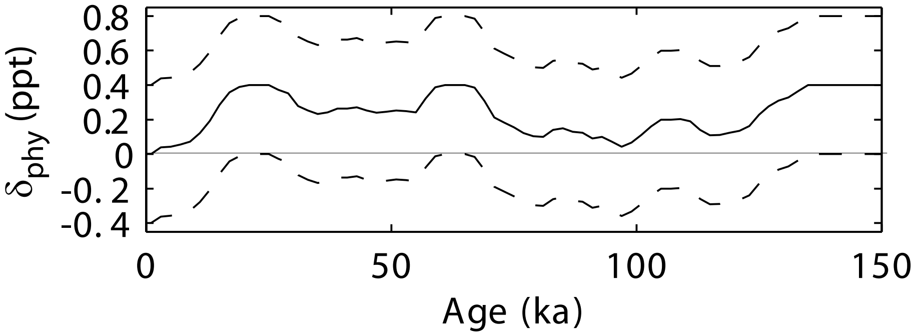

Fig. 4. Phyto-detritus correction and error, as a function of time, applied to selected cores, defined in Table 1.

CPD
5, 2497–2554, 2009

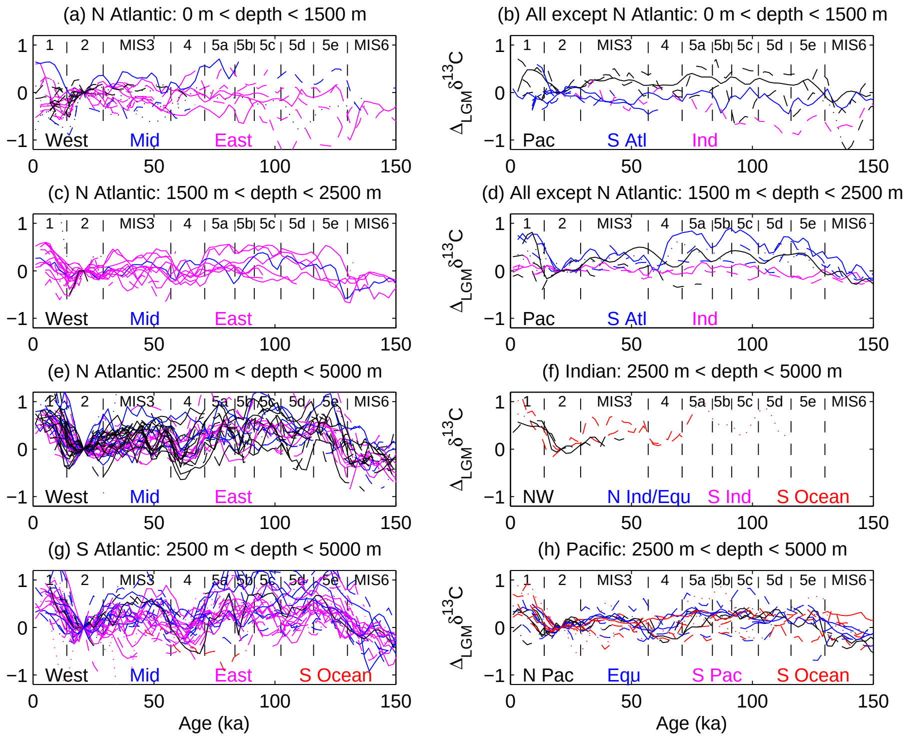

Fig. 5. Benthic $\Delta_{LGM}\delta^{13}C$ ($\delta^{13}C$ as an anomaly relative to the 21 ka value) time-series by region. Error estimates are <0.25‰ (solid), <0.5‰ (dashed), <0.8‰ (dotted); data with larger error estimates are not plotted. Colours indicate sub-regions: meridional boundaries are at 20° W and 0° W (N. Atlantic); 40° W and 20° W (S. Atlantic); 75° E (Indian). Equatorial cores are within 8° of the Equator. Marine Isotope Stages are indicated in each panel.

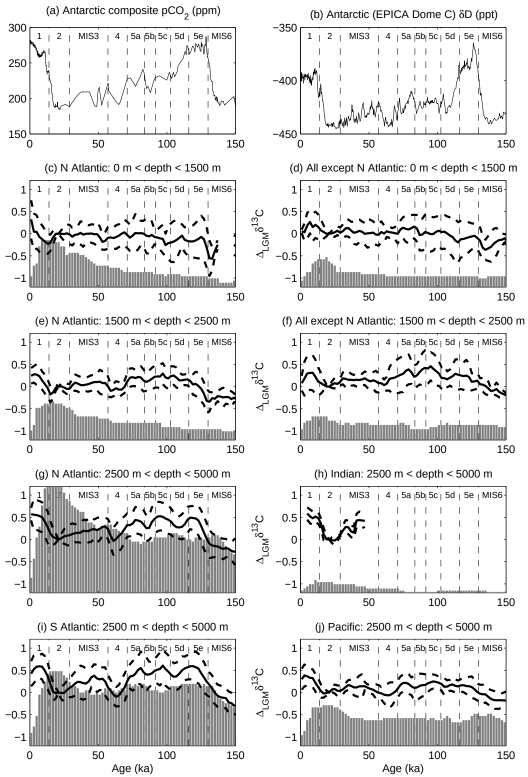

Fig. 6. Mean and standard deviation, weighted by the square of the inverse of the error estimate, of benthic $\Delta_{LGM}\delta^{13}C$ in each region. The histogram indicates the number of records used; where this is fewer than three, no data are plotted. Upper two panels show Antarctic CO_2 (Petit, 1999; Monnin et al., 2001) and deuterium (a proxy for temperature; EPICA community members, 2004) reconstructions for comparison; note the timescales for the marine and ice-core data are not homogeneous.

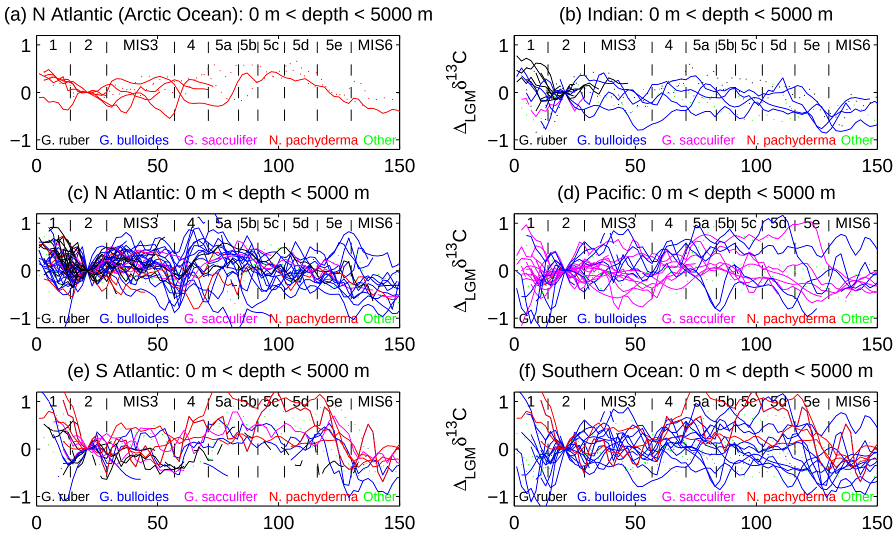

Fig. 7. Planktonic $\Delta_{LGM}\delta^{13}C$ time-series by region. Error estimates are <0.5‰ (solid), <0.6‰ (dashed), <0.8‰ (dotted); data with larger error estimates are not plotted (note these thresholds are different from thresholds for benthic data). Colours indicate planktonic species: *G. ruber* (black); *G. bulloides* (blue); *G. sacculifer* (magenta); *N. pachyderma* (red); other (green).

CPD

5, 2497–2554, 2009

Title Page
Abstract
Introduction
Conclusions
References
Tables
Figures
◀◀
▶▶
◀
▶
Back
Close
Full Screen / Esc
Printer-friendly Version
Interactive Discussion

CPD

5, 2497–2554, 2009

Synthesis of marine $\delta^{13}C$

K. I. C. Oliver et al.

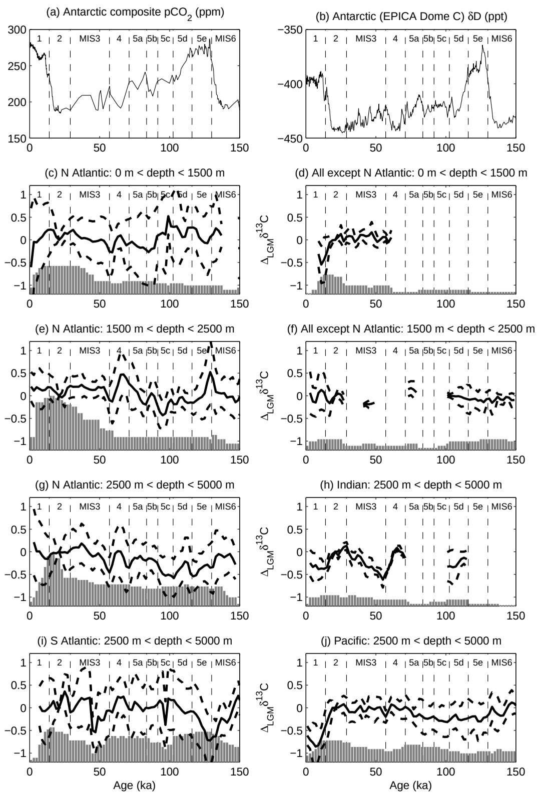

Fig. 8. Mean and standard deviation, weighted by the square of the inverse of the error estimate, of planktonic minus benthic $\Delta_{LGM}\delta^{13}C$ in each region. The histogram indicates the number of records used; where this is fewer than three, no data are plotted. Upper two panels show Antarctic CO_2 (Petit, 1999; Monnin et al., 2001) and deuterium (a proxy for temperature; EPICA community members, 2004) reconstructions for comparison; note the timescales for the marine and ice-core data are not homogeneous.

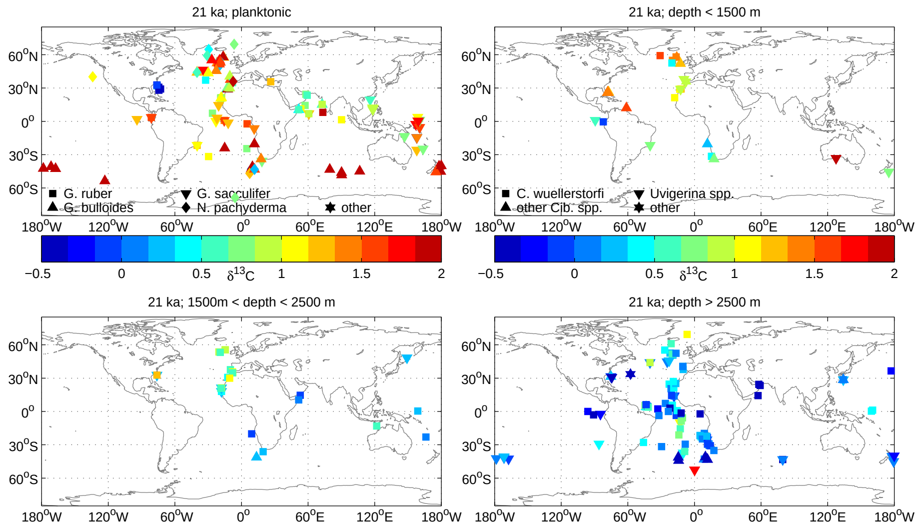

Fig. 9. 21 ka (LGM) δ^{13}C time-slice for planktonic species (top left) and benthic species (other panels). Only planktonic data with an error <1.0‰ and benthic data with an error <0.8‰ are plotted.

CPD

5, 2497–2554, 2009

Synthesis of marine $\delta^{13}C$

K. I. C. Oliver et al.

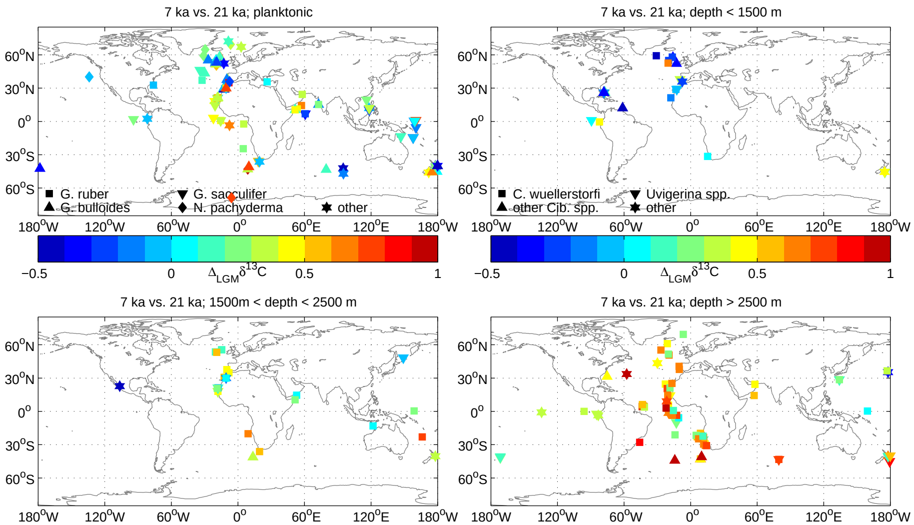

Fig. 10. 7 ka $\Delta_{LGM}\delta^{13}C$ ($\delta^{13}C$ as an anomaly relative to the 21 ka value) time-slice for planktonic species (top left) and benthic species (other panels). Only planktonic data with an error <0.8‰ and benthic data with an error <0.65‰ are plotted.

CPD
5, 2497–2554, 2009

Synthesis of marine $\delta^{13}C$

K. I. C. Oliver et al.

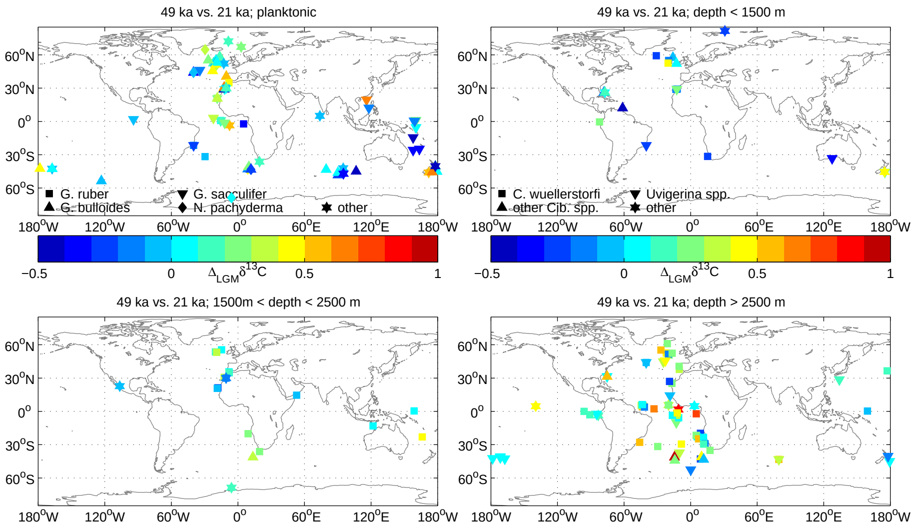

Fig. 11. 49 ka $\Delta_{LGM}\delta^{13}C$ ($\delta^{13}C$ as an anomaly relative to the 21 ka value) time-slice for planktonic species (top left) and benthic species (other panels). Only planktonic data with an error <0.8‰ and benthic data with an error <0.65‰ are plotted.

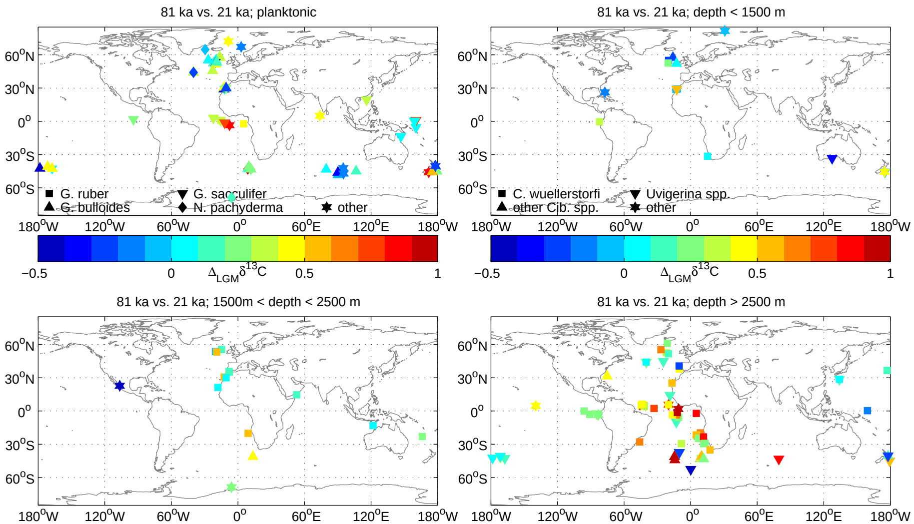

Fig. 12. 81 ka $\Delta_{LGM}\delta^{13}C$ ($\delta^{13}C$ as an anomaly relative to the 21 ka value) time-slice for planktonic species (top left) and benthic species (other panels). Only planktonic data with an error <0.8‰ and benthic data with an error <0.65‰ are plotted.

CPD
5, 2497–2554, 2009

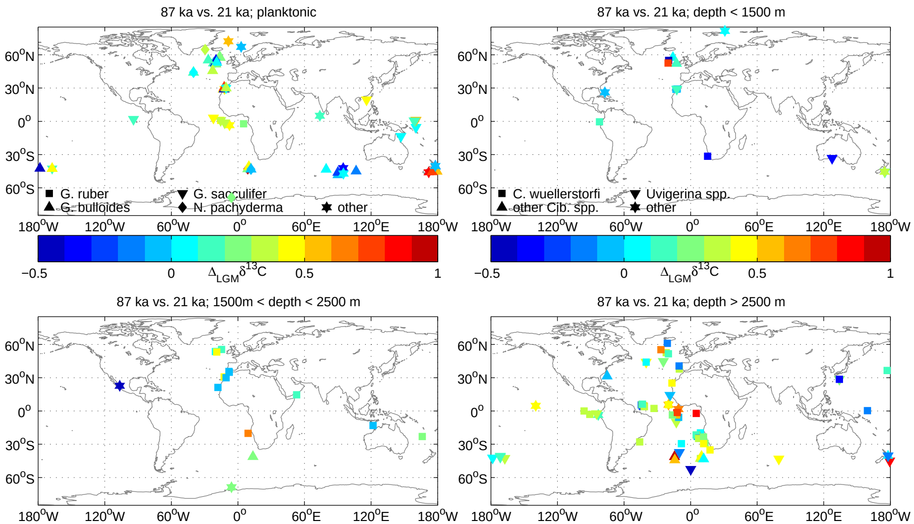

Fig. 13. 87 ka $\Delta_{LGM}\delta^{13}C$ ($\delta^{13}C$ as an anomaly relative to the 21 ka value) time-slice for planktonic species (top left) and benthic species (other panels). Only planktonic data with an error <0.8‰ and benthic data with an error <0.65‰ are plotted.

CPD

5, 2497–2554, 2009

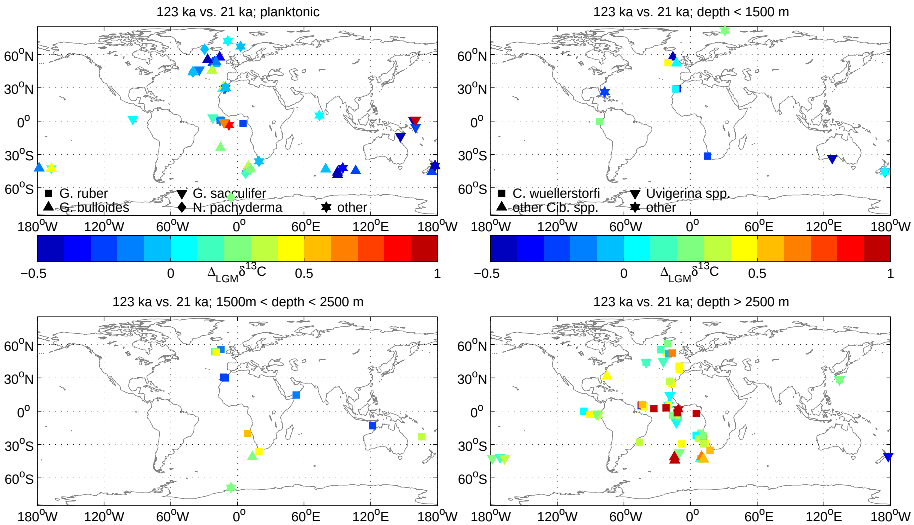

Fig. 14. 123 ka $\Delta_{LGM}\delta^{13}C$ ($\delta^{13}C$ as an anomaly relative to the 21 ka value) time-slice for planktonic species (top left) and benthic species (other panels). Only planktonic data with an error <0.8‰ and benthic data with an error <0.65‰ are plotted.